Published in final edited form as:
Nat Microbiol. 2020 October 01; 5(10): 1207–1216. doi:10.1038/s41564-020-0745-6.

Targeting the trypanosome kinetochore with CLK1 protein kinase inhibitors

Manuel Saldivia[1,2], **Eric Fang**[3], **Xiaolei Ma**[3], **Elmarie Myburgh**[4], **Juliana B. T. Carnielli**[1], **Christopher Bower-Lepts**[1], **Elaine Brown**[1], **Ryan Ritchie**[5], **Suresh B. Lakshminarayana**[2], **Yen-Liang Chen**[2], **Debjani Patra**[2], **Elizabeth Ornelas**[3], **Hazel X. Y. Koh**[2], **Sarah Williams**[3], **Frantisek Supek**[6], **Daniel Paape**[5], **Richard McCulloch**[5], **Marcel Kaiser**[7,8], **Michael P. Barrett**[5], **Jan Jiricek**[2], **Thierry T. Diagana**[2], **Jeremy C. Mottram**[*,1], **Srinivasa P.S. Rao**[*,2]

[1]York Biomedical Research Institute, Department of Biology, University of York, UK [2]Novartis Institute for Tropical Diseases, USA [3]Novartis Institutes for Biomedical Research, USA [4]York Biomedical Research Institute, Hull York Medical School, University of York, UK [5]Institute of Infection, Immunity and Inflammation, University of Glasgow, UK [6]Genomics Institute of the Novartis Research Foundation, USA [7]Swiss Tropical and Public Health Institute, Switzerland [8]University of Basel, Switzerland

Abstract

The kinetochore is a macromolecular structure that assembles on the centromeres of chromosomes and provides the major attachment point for spindle microtubules during mitosis. In *Trypanosoma brucei* the proteins that make up the kinetochore are highly divergent, with the inner kinetochore comprising at least 20 distinct and essential proteins (KKT1-20) that include four protein kinases, CLK1 (KKT10), CLK2 (KKT19), KKT2 and KKT3. We report the identification and characterisation of the amidobenzimidazoles (AB) protein kinase inhibitors that have nanomolar potency against *T. brucei* bloodstream forms, *Leishmania* and *Trypanosoma cruzi*. Target deconvolution using a selection of 29 *T. brucei* mutants that over-express known essential protein kinases identified CLK1 as a primary target. Biochemical studies and the co-crystal structure of CLK1 in complex with AB1 show that the irreversible competitive inhibition of CLK1 is dependent on a Michael acceptor forming an irreversible bond with C215 in the ATP binding pocket, a residue that is not present in human CLK1, thereby providing selectivity. Chemical

[*]Corresponding authors: Correspondence to Jeremy Mottram and Srinivasa P.S. Rao., jeremy.mottram@york.ac.uk; srinviasa.rao@novartis.com.

Contributions

J.C.M, T.T.D and S.P.S.R planned the studies. Compounds synthesis, compound docking, PK assays, and library screening by H.X.Y.K, D.P, Y.L.C, S.B.L, S.W, F.S and J.J; HAT animal studies by E.M, R.R, M.P.B and M.K; generation of individual protein kinase cell lines by E.B and M.S; Compound target deconvolution, TbCLK1 functional characterisation, immunofluorescences and data analysis were performed by M.S and J.B.T.C.; protein recombinant production, kinase assays and mass spectrometry by E.F, De.P, C.B-L and M.S; Crystallization and structure determination by E.O, X.M.;CLK1 mutants plasmids designed and prepared by M.S, Da.P and R.M; J.C.M, S.P.S.R, and M.S prepared and wrote the manuscript. All authors reviewed, edited and approved the paper. J.C.M, S.P.S.R, M.P.B and T.T.D obtained funding.

Competing interests

The authors declare no competing interests, except that some authors have shares in Novartis.

Europe PMC Funders Author Manuscripts

Europe PMC Funders Author Manuscripts

inhibition of CLK1 impairs inner kinetochore recruitment and compromises cell cycle progression, leading to cell death. This work highlights a unique drug target for trypanosomatid parasitic protozoa and a new chemical tool for investigating the function of their divergent kinetochores.

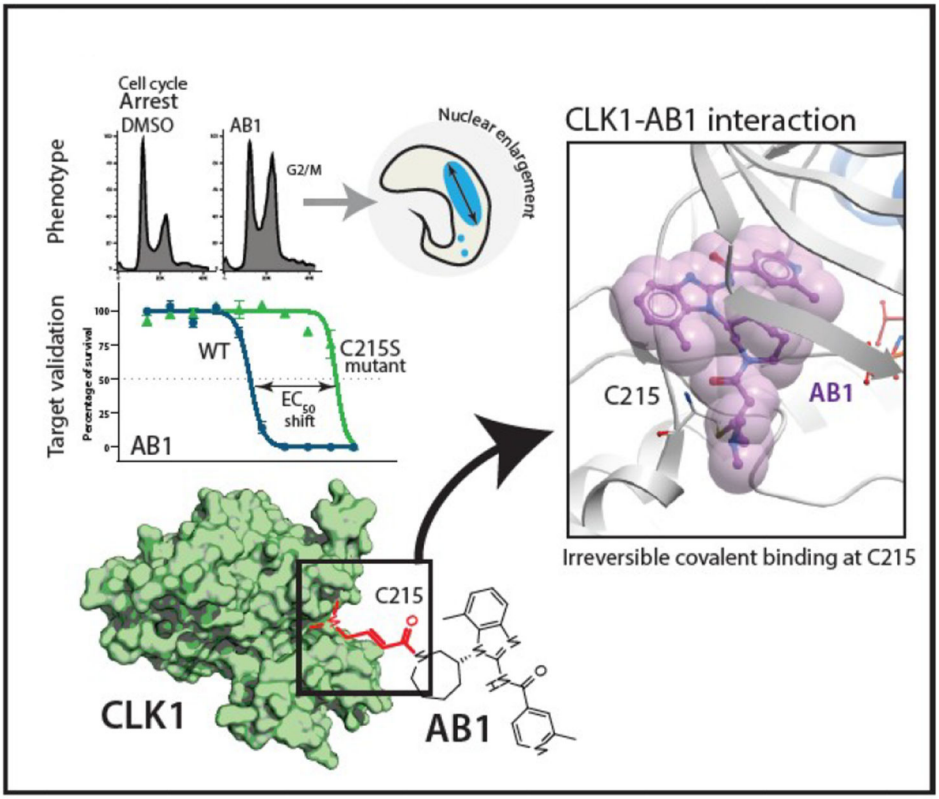

The three kinetoplastid neglected tropical diseases; leishmaniasis, Chagas disease, and human African trypanosomiasis (HAT) remain a significant global health burden. Over a billion people living in endemic regions are at risk from these neglected diseases with an estimated 30,000 deaths annually (WHO)[1]. While there have been notable recent advances in disease control, current therapies have severe shortcomings and there is an urgent need for innovative treatments that are safe, efficacious and easy to administer. Some of the significant advances include the development of novel oral therapy for sleeping sickness[2,3] and identification of pre-clinical candidates for leishmaniasis[4–6]. In order to find additional growth inhibitors, a whole parasite based phenotypic screen was carried out using ~2.3 million compounds against bloodstream forms of *T. brucei* [4], which included the Novartis kinase focused inhibitor library. This led to the identification of AB0, an Amidobenzimidazole (Fig. 1a and Supplementary Figure 1a) with an EC_{50} of 290 nM in an *in vitro T. brucei* parasite growth inhibition assay (Fig. 1a).

Detailed structure activity relationship (SAR) studies using ~250 close analogs obtained from the Novartis compound archive and focused medicinal chemistry efforts were carried out. The growth inhibition activity of compounds against *T. brucei* ranged 3 log orders with many compounds showing < 100 nM potency. Results also showed that the analogs having Michael acceptor chemical functionality are critical for potent activity and afford higher

lipophilic efficiency (LipE >3) required for more favourable drug-like properties (Fig. 1b, Supplementary Table 1). SAR analysis also led to the identification of more potent bioactive compounds, including AB1 (EC_{50} of 72 nM against *T. brucei*), with a >100-fold cytotoxicity window (Fig. 1a). AB1 not only showed potent activity against *T. b. gambiense* and *T. b. rhodesiense*, the causative agents of sleeping sickness but also had pan-kinetoplastid activity against *T. cruzi* (aetiology for Chagas disease), *Leishmania mexicana* (cutaneous leishmaniasis) *and L. donovani* (visceral leishmaniasis) suggesting that the molecular target is conserved across trypanosomatids (Fig. 1a). Compound AB1 was cidal to *T. brucei* showing concentration and time dependent kill, further it also exhibited relapse free cidality in wash-off assays suggesting ability to achieve sterile cure (Extended data Fig. 1b, c). In vitro wash-off assays are presumed to be predictive of compounds' ability to achieve relapse free cure in the mouse model of infection. AB1 had better solubility and *in vitro* pharmacokinetic properties with moderate to low clearance in mice, rat and human microsomes (Fig. 1a), allowing us to evaluate the ability to cure *T. brucei* infection in mouse models.

In vivo efficacy of AB1 was tested in mice with haemolymphatic and central nervous system (CNS) *T. brucei* infections using both STIB795 and GVR35 optimised bioluminescence HAT mouse models[7]. A dose dependent cure was observed with AB1, resulting in relapse free cure with a daily oral dosage of 50 mg/kg for four consecutive days in the STIB795 haemolymphatic mouse model of infection (Fig. 1c). However, despite a 4 log reduction in parasitaemia observed in a pleomorphic GVR35 strain chronic (CNS) model of infection, the parasitemia relapsed, most likely due to poor access of AB1 to parasites in the brain (Extended data Fig. 2a,b). Although AB1 showed good brain partitioning (measured brain to plasma ratio was 0.5), due to high brain tissue binding (>99%), the free fraction available for acting against the parasites in the brain was negligible, leading to poor efficacy (Extended data Fig. 2c,d). Further medicinal chemistry optimization is required to find compounds with better pharmacokinetic properties in order to achieve cure in the CNS model. The mouse efficacy studies using AB1 showed *in vivo* chemical validation of AB series compounds as promising anti-trypanosomatid candidates.

AB1 is a known covalent inhibitor of mutant human epidermal growth factor receptor (hEGFR) kinase, a well-studied target for non-small cell lung cancer (Fig 1a)[8]. Whilst hEGFR belongs to the tyrosine kinase family, the *T. brucei* genome lacks members of the receptor-linked or cytosolic tyrosine kinase families[9]. A major challenge for phenotypic hits is to identify the molecular target that is responsible for that effect. Since AB series compounds were hypothesized to target protein kinases, we generated inducible *T. brucei* gain-of function mutants of individual protein kinases to screen for resistance to AB1 (Fig. 2a). Twenty-nine essential protein kinases that had been assessed previously by RNAi as having specific RNAi induced cell cycle defects in bloodstream forms (BSF)[10] were analysed. In our screen, only one protein kinase, CLK1, showed a significant 6.5-fold increase in resistance compared with its uninduced control (Fig. 2b). In general over-expression of protein kinases show moderate resistance to their inhibitors. Wyllie and co-workers showed that co-over expression of CYC9 and wild type CRK12 in *L. donovani* resulted in 3-fold shift in cellular EC_{50} against the compound **5** (DDD853651/

GSK3186899), validating CRK12 as the target[5]. Over-expression of PI4K (phosphatidylinositol 4-kinase) in *Plasmodium falciparum* also rendered moderate 3-fold shift in EC_{50} against imidazopyrazine compounds, confirming the on-target effect[11].

In mammals, CLK1 belongs to the Clk (Cdc2-like kinase) family implicated in RNA splicing control and consists of at least four members[12]. In *T. brucei*, CLK1 is a kinetochore component essential for mitosis and has been proposed to be one of the potential targets for the fungal antibiotic hypothemycin[13–15]. As treatment with AB1 resulted in a G2/M cell cycle arrest (Fig. 2c-e) with most of the treated cells having an enlarged nucleus (Fig. 2d) similar to CLK1 RNAi knockdown (Extended data Fig. 3a-c), we tested if overexpression of CLK1 would confer resistance to drug-induced G2/M cell cycle arrest. Indeed, parasites overexpressing CLK1 had a normal cell cycle profile after treatment with AB1, in comparison to the parental cell line and DMSO uninduced control, which were G2/M arrested after treatment (Fig. 2c). CLK1 overexpression impairs parasite fitness without affecting cell cycle progression, suggesting that *T. brucei* tightly regulates CLK1 expression (Extended data Fig. 3d). In addition, AB1 attenuates CLK1 toxicity caused by over-expression, providing further evidence that CLK1 is the compound's primary target (Extended data Fig. 3e, f).

We expressed recombinant TbCLK1 and human CLK1 and tested ~230 compounds from the AB series to determine the biochemical SAR. Apparent IC_{50} was determined after 10 min post-incubation with the enzyme. A strong correlation was observed between inhibition of the *T. brucei* CLK1 enzyme and cellular activity (Pearson' correlation r = 0.68), supporting the chemical validation of CLK1 as the molecular target for the amidobenzimidazole series of compounds (Fig. 3a, Supplementary Table 1). The majority of the compounds showed greater selectivity against TbCLK1 compared to hCLK1 (Fig. 3b, Supplementary Table 1). AB1 inhibited TbCLK1 with an apparent IC_{50} of 10 nM, with 90-fold selectivity observed over hCLK1 (Fig. 3b). *T. brucei* also has another protein kinase, CLK2, which is closely related to CLK1, with 92% overall sequence identity and 100% identity in the protein kinase domain. CLK2 is less abundant than CLK1 in bloodstream forms (Extended data Fig. 4a, b). AB1 would be expected to inhibit the kinase activity of CLK2, but this is unlikely to contribute to killing in bloodstream forms of the parasite as CLK2-specific RNAi suggests the protein is not essential[13].

Interestingly, all compounds with a Michael acceptor inhibited TbCLK1 kinase activity but not others, strongly suggesting this functionality is an essential feature of the pharmacophore (Fig. 3a). In order to test the putative critical role played by the Michael acceptor, a compound similar to AB1, which has a saturated double bond at the Michael acceptor, was profiled in both enzymatic and cellular assays. This compound (AB2) was completely inactive in both TbCLK1 enzyme (apparent IC_{50} > 20 μM) and whole cell growth inhibition assays (Tbb EC_{50} > 50 μm), confirming the importance of the Michael acceptor for activity (Supplementary Table 1). The hEGFR inhibitors having Michael acceptors are known to covalently interact with an active site cysteine (C797) near the ATP binding domain[8,16].

In order to directly visualize the binding mode, structure of TbCLK1 kinase domain bound to AB1 was determined to 2.7Å (PDB 6Q2A) (Fig. 3c). At this resolution, the electron

density map has continuous density between the side-chain of the thiol group of C215 and the Michael acceptor of the inhibitor (Fig. 3c, d), strongly indicating the formation of an irreversible covalent bond between them. Furthermore, AB1 forms direct hydrogen bonds with the backbone amide NH of Y212 and C215 and a salt bridge with D218 (Fig. 3c), consistent with the binding mode of AB1 when covalently attached to hEGFR[8]. While both hEGFR and TbCLK1 have cysteine in their active sites, hCLK1 lacks cysteine and instead has serine in the same position (Extended data Fig. 5a-c). This has led to achieving significant selectivity for most AB series compounds for TbCLK1 (Fig. 3b). Beyond the AB1 binding site, the TbCLK1 kinase domain exhibits an overall structure that is in line with a kinase in the active conformation, closed kinase lobes, a well-ordered activation loop, DLG-in and an intact salt bridge to αC-helix (Fig. 3c).

To investigate the covalent binding and interaction with C215, we co-incubated AB1 and AB2 with both wild type and C215A mutant of TbCLK1 and assessed the interaction using biophysical methods. As expected, incubation of AB1 with wild type TbCLK1 enzyme resulted in a 12° C shift in denaturing temperature as seen by differential scanning fluorimetry (Fig. 4a and Extended data Fig. 6a). Similarly, mass spectrometric analysis also showed one main product per protein which has an average mass 475 Da higher than the unmodified protein (Extended data Fig. 6b). This was consistent with the addition of one molecule of AB1, which has a mass of 475 Da. No shift in the mass was seen for AB2, or in C215A mutant CLK1 (Extended data Fig. 6a). These results clearly show covalent interaction of the Michael acceptor with C215 of TbCLK1. In addition, TbCLK1 C215A is not inhibited by AB1, but is inhibited by the non-covalent pan-kinase inhibitor staurosporine (Fig. 4b). Multiple sequence alignment of CLK1 from *T. brucei*, *T. cruzi* and *L. mexicana* showed high sequence similarity and C215 was conserved across parasites, further suggesting the growth inhibition of these parasites by AB1 could be due to TbCLK1 inhibition (Extended data Fig. 4c).

Further, to assess the importance of *T. brucei* CLK1 C215 in AB1 binding in parasites, a recoded version of CLK1 that contained a Cys to Ala mutation at position 215 was expressed in the TbCLK1 RNAi line. In this cell line, RNAi induction depleted the wild type CLK1 mRNA but the recoded CLK1 C215A mRNA was not susceptible to RNAi-induced degradation and was expressed. This triggered a G2/M cell cycle arrest, suggesting this residue is important for CLK1 function and may mimic AB1 –TbCLK1 mediated inhibition. Since expression of the C215A mutation affected the fitness of the parasites, we attempted to express a C215S mutation, as human CLK1 has serine at position 215. Parasites expressing the TbCLK1 C215S mutation had a normal cell cycle profile (Extended data Fig. 7a, b) and were resistant to treatment with 5x EC_{50} of AB1 (Extended data Fig. 7c). Thus, we evaluated if the overexpression of the C215S mutation in the parental cell line increased this resistance, and indeed, this mutation conferred a > 60-fold EC_{50} shift of resistance against AB1 (Fig. 4c), which also significantly reduced the effect of AB1 in the parasite's growth and survival (Fig. 4d, e). Interestingly, we observed that AB1 treatment induced a mobility shift on CLK1, which likely corresponds to phosphorylation, whilst the C215S mutant protein remained unaltered (Extended data Fig. 7d). Together, these data demonstrate target engagement in the parasite and inhibition of CLK1 with AB1.

TbCLK1 (KKT10) is a core component of the inner kinetochore. In other organisms, the kinetochore supports directional movement of chromosomes into microtubules to ensure faithful chromosome segregation[17]. Some of the *T. brucei* kinetochore components have been recently described, and grouped according to their patterns of expression/localization through the cell cycle[14,18]. The significant divergence between components of the human and parasite kinetochores underpins its potential druggability. Although depletion of TbCLK1 has been associated with the presence of lagging chromosomes during mitosis in procyclic cells[14] the causal link of TbCLK1 to this process has yet to be established. To investigate this further *T. brucei* bloodstream form cells were synchronised by cell sorting[19] to give 2C and 4C nuclear DNA content populations and then allowed to enter the cell cycle in the presence or absence of AB1 (Fig 2e and Extended data Fig. 8 a-c). Inhibition of TbCLK1 in the 2C population (G1-phase) synchronously progressing through the cell cycle led to arrest of cells in late metaphase with a 2K1N configuration (defined as cells having 2 kinetoplasts (2K) and 1 nucleus (1N)). By contrast, inhibition of TbCLK1 in the 4C population synchronously progressing through the cell cycle induced an arrest in the late anaphase (2K2N population). These data are consistent with inhibition of TbCLK1 causing a disruption in kinetochore function during metaphase and exit from anaphase into cytokinesis. To confirm this, we tagged KKT2, a canonical centromere kinetochore protein, with mNeonGreen and assessed its localisation in the presence and absence of AB1. Similar to previous observations in procyclic form cells[14,18], we observed in bloodstream form cells that KKT2 is constitutively expressed until anaphase. Treatment with either 2 x EC_{50} of AB1 for 24 hr or 5 x EC_{50} of AB1 for 6 hr caused dispersal of the defined foci of the kinetochore within the nucleus (Fig. 5a). This change of KKT2 pattern was also observed after depletion of CLK1 by RNAi (Fig. 5b). These data demonstrate that inhibition of CLK1 by AB1 causes impairment of kinetochore function thereby defining a consequence of AB1 treatment.

Discussion

Our studies indicate that the principal mechanism of action for the amidobenzimidazole series is inhibition of the trypanosome CLK1 protein kinase. In support of this, we show for over 230 compounds that a strong correlation exists between inhibition of recombinant TbCLK1 and killing of the parasite. Only those compounds that have a Michael acceptor and are predicted to form a covalent bond with C215 of CLK1 are active and the X-ray structure, differential scanning fluorimetry and mass spectrum chromatograms clearly demonstrate the covalent linkage for AB1. We also show that over-expression of CLK1 or the CLK1 C215S mutant provide 6.5-fold or >60-fold resistance of the parasite to AB1, respectively, demonstrating target engagement. AB1 treatment of bloodstream form trypanosomes lead to chromosome mis-segregation and cell cycle arrest, consistent with inhibition of CLK1, which is a kinetochore kinase (KKT10). Generation of parasites resistant to compounds and the identification of mutations in target genes is a well-established method for target deconvolution[4,5]. However, we failed to generate parasites resistant to AB1, even after a year and half under compound selection. This might be explained if AB1 has an element of polypharmacology and one potential secondary target is CLK2, which is an active enzyme[20] and has an identical protein kinase domain to CLK1,

thus inhibited by AB1. In procyclic form trypanosomes CLK1 and CLK2 are functionally redundant[21], whilst in bloodstream form parasites CLK1 is essential, but CLK2 is not essential[15,22]. An explanation for this arises from our finding that CLK1 is more highly expressed than CLK2 in bloodstream forms, such that inhibition of CLK1 activity leads to chromosome mis-segregation and cell cycle arrest, phenotypes consistent with inhibition of a kinetochore kinase (KKT10).

We propose that inhibition of CLK1 activity with AB1 leads to impaired kinetochore function and irreversible arrest in metaphase leading to cell death. A combination of growth inhibition screening, target identification and characterization resulted in the chemical validation of CLK1 as a unique pan-kinetoplastid drug target. In recent years six covalent inhibitors of protein kinases have been successfully approved for cancer treatment[23], underlining the possibility of developing covalent inhibitors into drugs. The combination of a distinct mechanism of action targeting the kinetochore, and a new series of antitrypanosomatid AB compounds, which have reduced chances of acquiring resistance in the clinic, add to the proteasome and CRK12 inhibitors already entering clinical trials[4,5,24,25]. One of the key challenges for the AB series of compounds to progress to the clinic is to improve kinase selectivity and the co-crystal structure determined in the current study will significantly help in structure based medicinal chemistry optimization to resolve this issue. The current efforts of CLK1 target validation also open up opportunities for focused structure-based drug design using fragment screens in order to obtain non-covalent inhibitors that have pan-kinetoplastid growth inhibition properties. In addition, the high level of sequence divergence of trypanosome kinetochore complex proteins from humans[14,26] make the kinetochore a high value target.

Methods

Cellular assays

A kinase focused inhibitor library (containing approximately 10,000 compounds) was screened at a single concentration of 10 μM for the ability of compounds to inhibit growth of *T. b. brucei* Lister 427. This resulted in 2264 compounds showing > 50% growth inhibition. Chemi-informatic analysis of hits resulted in ~200 clusters, representatives of these were subjected to 10-point dose-response growth inhibition assays against bloodstream form of *T. b. brucei* Lister 427. Further removal of non-favourable chemical structures such as nitrofuranes, cytotoxicity profiling using the HepG2 cell line (selectivity index of 10) and favourable physico-chemical properties (polar surface area <100; molecular weight <500 and lipophilicity <4.5) led to identification of an amidobenzimidazole scaffold (AB0) for further follow up.

Bloodstream form of *Trypanosoma brucei brucei* Lister 427, *T. b. gambiense* STIB930 and *T. b. rhodesiense* STIB900 were cultured in HMI-9 medium as described elsewhere[4]. Other kinetoplastid parasites *Leishmania donovani* HU3 and *L. mexicana* (MNYC/BZ/62/M379) were cultured in RPMI 1640 media as described earlier[4,27]. The *T. cruzi* Tulahuen parasites constitutively expressing *Escherichia coli* β-galactosidase[28] were maintained in tissue culture as an infection in NIH 3T3 fibroblast cells[4]. NIH 3T3 and human epithelial (HepG2) cells were obtained from ATCC and grown in RPMI media (Life Technologies).

All other transgenic *T. b. brucei* parasites used in this study were derived from monomorphic *T. b. brucei* 2T1 bloodstream forms[29] and were cultured in HMI-11 [HMI-9 (GIBCO)containing 10% v/v foetal bovine serum (GIBCO), Pen/Strep solution (penicillin 20 U ml^{-1}, streptomycin 20 mg ml^{-1})] at 37 °C/5% CO_2 in vented flasks. Selective antibiotics were used as follows: 5 μg ml^{-1} blasticidin or hygromycin and 2.5 μg ml^{-1} phleomycin or G418. RNAi or overexpression was induced *in vitro* with tetracycline (Sigma Aldrich) in 70% ethanol at 1 μg ml^{-1}. Endogenous Ty, mNeonGreen or myc overexpression tagging were performed using the pPOTv6 vector[30] and pRPa[29], respectively. The generation of inducible TbCLK1 RNAi was generated as previously described[13]. All primers are listed in Supplementary methods Table 1.

All cell based assays were performed as described before[4,31]. Briefly, bloodstream form of *T. b. brucei Lister* 427, *T. b. rhodesiense* and *T. b. gambiense* parasites were incubated with varying concentration of compounds for 48 hr. Cell viability was assessed by measuring ATP levels using CellTiter-Glo reagent (Promega) and 50% growth inhibition (EC_{50}) was calculated using sigmoidal dose response curves. For both intracellular *T. cruzi* amastigotes and *L. donovani* HU3 axenic amastigotes growth inhibition was measured as described earlier[4]. Intracellular *L. mexicana* amastigote growth inhibition was assessed by microscopy. Briefly, after primary peritoneal mouse macrophages were infected with late-log-phase promastigotes at an infection ratio of 10:1; non-internalized parasites were removed by washing the plates with PBS, and cells were cultured with different drug concentrations for 96 hr. Determination of intracellular parasite numbers were done by fixing the cells in methanol and then stained with DAPI. Cytotoxicity (CC_{50}) was also measured against mouse fibroblast NIH 3T3 and HepG2 cell lines by incubating compounds for 4 days[4].

Single protein kinase overexpression lines (Supplementary methods table 1) were generated by transfecting *T. brucei brucei* 2T1 cells with a tetracycline inducible overexpression plasmid linearized with *Asc*I restriction enzyme. Each overexpression construct contains the open reading frame (ORF) of a single protein kinase in the plasmid pGL2220 (pRPaiMYCx)[32]. This plasmid integrates at the tagged rRNA spacer (single locus) of 2T1 *T. brucei*.

Protein kinase overexpression cell lines were adjusted to 2×10^5 cells ml^{-1} and induced for 18 hr by the addition of tetracycline to a final concentration of 1 μg ml^{-1} in 70% ethanol. To establish the EC_{50}, the protein kinase overexpression cell lines and parental control 2T1 were treated with two-fold increasing concentrations of compounds (with similar DMSO increasing concentration as control). Cell viability was measured at 48 hr with a POLARstar Omega plate reader spectrophotometer; the determination of cell viability was carried out by the established colorimetric technique using Alamar Blue (0.49 mM resazurin in phosphate-buffered saline (PBS)), in a 96-well plate format spectrophotometric assay which measures the ability of living cells to reduce resazurin. We used pentadimine isethionate (Sigma Aldrich) as a positive control. Fluorescence emission was detected using a CLARIOstar ® reader (BMG LABTECH; excitation filter at 540 nm and emissions filter at 590 nm). Fitting of dose-response curves and IC_{50}/EC_{50} determination were normalized as percentage of inhibition based on controls. Hesperadin was obtained from ApexBio Technology.

Mouse infection models for *T. brucei*

The *T. brucei* strain STIB795 acute mouse model mimics the first stage of African trypanosomiasis[33]. Six female NMRI mice were used per experimental group, divided into two cages (A and B). Each mouse was inoculated by intraperitoneal injection with 10^4 bloodstream forms of STIB795, respectively. Heparinized blood from a donor mouse with approximately 5 x 10^6 ml^{-1} parasitaemia was suspended in phosphate saline glucose (PSG) to obtain a trypanosome suspension of 1×10^5 ml^{-1}. Each mouse was injected with 0.25 ml. Compounds were formulated in 0.5% Tween80 in 0.5% methylcellulose. Compound treatment was initiated 3 days post-infection and administered orally on four consecutive days in a volume of 0.1 ml/10 g. Three mice served as infected-untreated controls. They were not injected with the vehicle alone since we have established in our labs that these vehicles do not affect parasitaemia nor the mice. Blood samples were taken after the 4th treatment. From the mice in cage A, -1 h, 2 h and 8 h after the 4th treatment, 20 uL of blood each were taken from the tail vein and from mice in cage B 1 h, 4 h, and 24 h after the 4th treatment. Parasitaemia was monitored microscopically by tail blood examination twice a week until 31 days post-infection. Mice were considered cured when there was no parasitaemia relapse detected in the tail blood over the 30-day observation period. *In vivo* efficacy studies in mice were conducted at the Swiss Tropical and Public Health Institute (Basel) (License number 2813) according to the rules and regulations for the protection of animal rights ("Tierschutzverordnung") of the Swiss "Bundesamt für Veterinärwesen". They were approved by the veterinary office of Canton Basel-Stadt, Switzerland.

Plasmids

Recoded *CLK1* was synthesised by Eurofins Genomics. The recoded CLK1 sequence (*CLK1*^{R}) codes for the same amino acid sequence as *CLK1* but only shares 95.06% nucleotide identity. All segments of identity between *CLK1* and *CLK1*^{R} are less than 20 base pairs long. *CLK1*^{R} was inserted by Gibson assembly® (New England Biolabs) into the plasmid pGL2492 using *Xba*I and *Bam*HI restriction sites, generating pGL2832. This plasmid is designed to constitutively express CLK1 from the tubulin locus, with the addition of a C-terminal 6x HA tag. To express the cysteine 215 mutants, the cysteine 215 was changed to serine or alanine by mutating pGL2832, carrying the coding sequence for *CLK1*, using site directed mutagenic PCR (Primer sequences in Supplementary methods). Similarly, C215S mutation was introduced into original CLK1 OE plasmid, to generate CLK1 C215S OE (NITD001 plasmid) into the parental 2T1 cell line.

Immunofluorescence, cell cycle analysis and cell sorting

Cells treated for 6 hr with compounds or DMSO were centrifuged at 1400 g for 10 min before washing twice with TDB-glucose at room temperature. Suspensions were centrifuged at 1000 g for 5 min and pipetted into 6-well microscope slides and dried at RT. Cells were fixed with 25µl 2% paraformaldehyde diluted in PBS and incubated at room temperature for 5 min. Cells were washed in PBS to remove paraformaldehyde prior to washing twice more with PBS and permeabilized with 0.05% NP40 for 10 min. Cells were washed twice in PBS and dried at RT. Mounting media with DAPI was added to each well with a coverslip. Slides

were kept at 4 °C before viewing using a Zeiss LSM 880 with Airyscan on an Axio Observer.Z1 invert confocal microscope.

For cell cycle analysis, bloodstream form *T. brucei* cell lines were incubated or not for 6 hr with AB compounds at a final concentration of 2X and 5X the individual EC_{50} value for each compound (averaged from viability assays). Control cultures were treated with 0.5µl DMSO but no AB compound. Cultures were pelleted and cells were collected and washed once in *Trypanosoma* dilution buffer (TDB) supplemented with 5 mM of EDTA and resuspended in 70% methanol. Cells were centrifuged at 1400 g for 10 min to remove methanol and washed once in TDB 1x with 5mM EDTA. Cells were resuspended in 1ml TDB 1x with 5mM EDTA, 10µg ml^{-1} of propidium iodide and 10µl of RNase A. Cell suspensions in 1.5 ml tubes were wrapped in foil to avoid bleaching by light. Cells were incubated for 30 min at 37°C in the dark until FACS analysis. Cells were analysed for FACS using a Beckman Coulter CyAn ADP flow cytometer (excitation; 535, emission; 617).

In the cell cycle analysis, CLK1 OE was induced during 18 hr with tetracycline (1 µg ml^{-1}) and later treated with 4X the individual EC_{50} value for each compound for 4 hr (maintaining tetracycline induction), and finally collected for flow cytometry as above.

Parasite cell sorting was conducted as described previously[19]. Briefly, cell lines were harvested during exponential growth by centrifugation for 10 min at room temperature. The parasite pellet was then resuspended at a concentration of 1×10^6 cells ml^{-1} in HMI-9 medium supplemented with 2% FCS and 10 µg ml^{-1} penicillin/streptomycin. Vybrant DyeCycle Violet (Molecular Probes, Invitrogen) was added to a final concentration of 1 µg $ml^{-1}$and the cell suspension incubated for 30 min at 37 °C, the tube being protected from light by wrapping in aluminium foil. The samples were then centrifuged and resuspended back in the staining media prior to sorting on a MoFlo XDP Sorter (Beckman Coulter Life Sciences). During and after the sorting, the samples were cooled to below 20 °C to limit cell metabolic activity. The dye was excited using a 407 nm Violet laser and emission detected via a 450/40 bandpass filter. Live parasites were gated based on FSC/SSC profiles, and the gates were set up to collect only the 2C fraction (G0/G1 cells) and 4C fraction (G2, mitotic and post-mitotic cells), to ensure efficient discrimination and selection of these cell-cycle stages.

Protein analysis

Biochemical assays for human EGFR (Epidermal growth factor receptor) and BTK (Bruton's tyrosine kinase) were carried out using a homogenous time-resolved fluorescence (HTRF) assay as described previously[8].

For enzyme purification, full-length TbCLK1 (Q382U0) CDS was cloned in pET28a PreSc-His and pET24-MBP-TEV vector respectively. Human CLK1 (hCLK1; P49759) was obtained from Promega. Recombinant expression was carried out by lactose autoinduction in Terrific Broth containing 0.4% glycerol, 0.05% glucose, 0.05% lactose, 0.05% arabinose and buffered by 100 mM sodium phosphate (pH 7.0). In brief, 0.7 L of this media (in a 2.8 L Fernbach flask) was inoculated at 0.1 OD600 with an overnight Luria Broth culture and shaken at 37 ˚C and 250 rpm for 2.5 hr. Then, temperature was lowered to 18 ˚C and the

culture was allowed to grow and induced overnight and harvested 20-24 hr later. Cells were pelleted and stored at -80 ˚C prior to purification. Cell lysis was done by sonication in an ice bath (20 sec ON/OFF, 3 min active sonication at 70-110 watts power) in 40 mL equilibration buffer (25 mM HEPES pH 7.5 300 mM NaCl 5% glycerol 0.5 mM TCEP) and the clarified lysate is purified by IMAC on a 5 mL HisTrap column (GE Healthcare). The IMAC elution was further purified by sizing on a 300 mL Superdex 200 prep grade column (GE Healthcare) packed in a 2.6 cm diameter housing. Included volume fractions were pooled and analysed by SDS-PAGE or LC-MS.

Preliminary characterization of the TbCLK1 enzyme was carried out and the Km for ATP and MBP (Myelin basic protein, dephosphorylated, Sigma-Aldrich Catalogue no: 13-110, LOT: 3107375) substrate was found to be 9.3 ± 3.6 μM and 0.065 ± 0.02 mg ml^{-1}, respectively. TbCLK1 and hCLK1 enzyme activity assays were performed in white 384 well, solid bottom, Small Volume™ plates (GREINER). The assay buffer contained 40 mM Tris (pH 7.5), 20 mM $MgCl_2$, 0.1mg/ml BSA and 2 mM DTT. Each enzyme (TbCLK1 = 3 nM; hCLK1 = 50 nM) was first incubated with different compound serial dilutions or DMSO control during 10 min and then ATP (10 μM) and MBP substrate (0.1 mg ml^{-1}) mixture was added to initiate the reaction. After 30 min reaction at room temperature, the ADP-Glo reagent and detection solution were added following the technical manual of ADP-Glo™ kinase assay kit (Promega). The luminescence was measured on CLARIOstar BMG LABTECH microplate reader. In all the assays, staurosporine was used as positive control of inhibition. Apparent IC_{50} values were plotted using GraphPad Prism software. The co-crystal structure of TbCLK1 with AB1 showed specific covalent interaction with cysteine 215. It may be possible that all AB series compounds with Michael acceptors have covalent inhibition of TbCLK1. Since biochemical SAR analysis for all AB series compounds was carried out beyond 10 min incubation with rCLK1, IC_{50}s are represented as apparent IC_{50}s. The AB1 compound showed time dependent inhibition of rCLK1 wherein IC_{50} plateaued around 20 min.

For Western blotting parasites were washed with trypanosome dilution buffer (TDB) supplemented with 20 mM glucose. After centrifugation, the samples were resuspended in the RIPA buffer (New England Biolabs) supplemented with protease and phosphatase inhibitors obtained from Promega and Roche Life Science respectively. All samples were quantified by *Bradford protein* assay (Bio-Rad), 25 μg of protein was loaded, resolved in a 4-20% NuPAGE Bis-Tris gel (Invitrogen) in NuPAGE MOPS running buffer and transferred onto Hybond-C nitrocellulose membranes (GE Healthcare) at 350 mA for 2 hr or, for high molecular weight proteins, overnight at 4 °C.

After transfer, membranes were washed once in 1x TBST (tris-*buffered* saline (TBS), 0.01% Tween-20 (Sigma Aldrich)) for 10 min then incubated for 1 hr in blocking solution (1x TBST, 5% BSA) or, if required, overnight at 4 °C. Next, the membrane was rinsed for 10 min in 1X TBST and placed in blocking buffer containing the required primary antisera for 1 hr at room temperature or overnight at 4 °C. The membrane was then washed 3 times with TBST and placed in blocking solution containing the appropriate fluorescent secondary antisera for 1 hr. A list of antibodies is provided in Supplementary Methods.

Determination of solubility, plasma protein binding, brain tissue binding and microsomal clearance

Solubility of AB0 and AB1 compounds were determined in a high-throughput thermodynamic solubility assay as described previously[34]. Plasma protein binding was determined for AB1 using mouse blood[34], whilst brain tissue binding was determined using rat brain tissues. Intrinsic metabolic clearance of AB0 and AB1 were determined in mouse, rat and human liver microsomes using the compound depletion approach and LC-MS/MS quantification[35].

Crystallization, data collection, and structure determination

The TbCLK1/AB1 complex was formed by incubating TbCLK1 kinase domain (V117-M465) with 1mM AB1 at room temperature for 2 hours. The excess AB1 was removed by dialysis overnight in buffer containing 25mM HEPES pH 7.5, 250mM NaCl, 0.5mM TCEP. The TbCLK1 kinase domain/AB1 complex was concentrated to 15 mg/ml for crystallization trials. Crystallization experiments were carried out at 4°C using the sitting-drop vapor diffusion setup. Crystals of the TbCLK1 kinase domain/AB1 complex grew out of a well containing 0.1M HEPES pH 7.5, 1.6M Ammonium Sulfate, 2% w/v Peg 1000. Crystals were cryo-protected in reservoir solution supplemented with 20% glycerol and flash-cooled in liquid nitrogen for data collection. Datasets were collected under cryogenic conditions (100K) at the Advanced Light Source (ALS) beamline 5.0.2. All data were processed using Xia2[36], employing XDS[37] for data integration and AIMLESS[38] for scaling. Molecular replacement were carried out using PHASER[39] with coordinates from human CLK1 crystal structure (PDB ID 6FT8)[40]. Structure refinement was carried out in PHENIX[41] alternated with manual fitting in Coot[42]. Data collection and structure refinement statistics are included in Extended data Table 1.

Differential Scanning Fluorimetry (DSF) for CLK1

Scanning fluorimetry (DSF) was performed on an Applied Biosystems Viia 7 RT PCR instrument, and data was analyzed using Protein Thermal Shift Software version 1.3 (Applied Biosystems/Thermo Fisher). Recombinant *Trypanosoma brucei* CLK1 wild-type or C215A protein was diluted to 5 μM in 25 mM 4-(2-Hydroxyethyl)piperazine-1-ethanesulfonic acid, N-(2-Hydroxyethyl)piperazine-N′-(2-ethanesulfonic acid) (HEPES) pH 7.5 300 mM NaCl 5% glycerol and 1 mM Tris(2-carboxyethyl)phosphine hydrochloride (TCEP). Compounds in DMSO or DMSO control was added to a final concentration of 2 mM DMSO and 50 uM compound. SYPRO Orange (Invitrogen/Thermo Fisher) was pre-diluted to 100x in the protein buffer and added to a final concentration of 10x. 70 ul of each condition was prepared. After 30 min of incubation, 3x 20 ul was aliquoted bubble-free into a 384 well PCR plate and covered with RT PCR compatible film, then centrifuged 10 min at 2000 rpm at room temperature, and read in the RT PCR instrument with the appropriate filters. The thermal shift program consisted of 3 minutes at 25 ˚C followed by a 25-95 ˚C ramp at 0.03 ˚C/second and 5 seconds at 95 ˚C.

General Statistics

All statistical analysis was performed using GraphPad Prism 8 (http://www.graphpad.com/scientific-software/prism/). The appropriate tests were conducted and are as detailed in the corresponding figure legends.

Extended Data

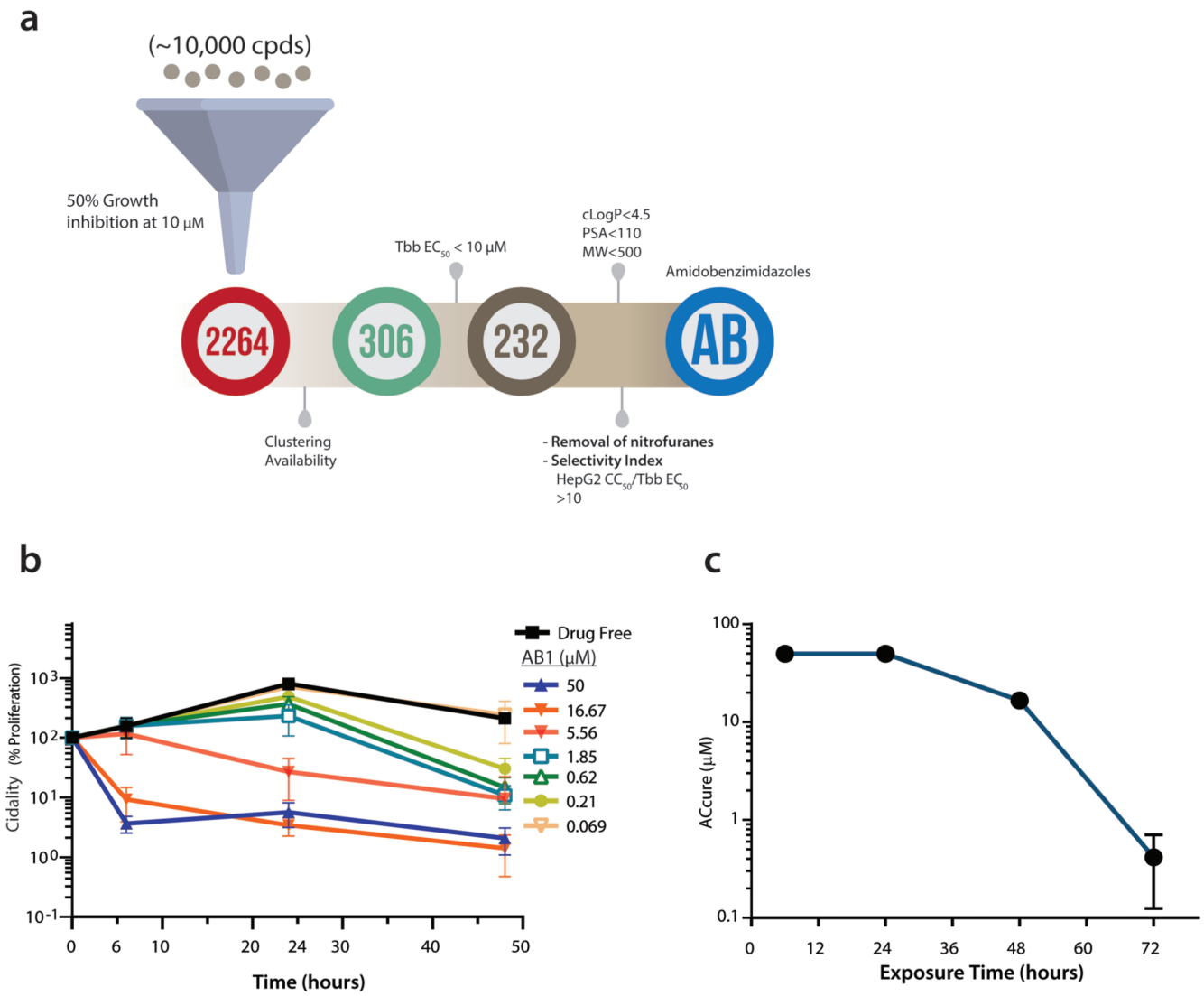

Extended Data Fig. 1. High-throughput screening of kinase library and characterization of AB1 effect on *T. brucei*.

(a) Identification of amidobenzimidazole (AB) series as a scaffold worthy of progression. Single point screen of ten thousand compounds from kinase library were screened against *T. b. brucei* parasite for growth inhibition at 10 μM. 2264 cpds showed >50% growth inhibition, of which 306 compounds were prioritized based on the cluster analysis and compound availability for 10 point dose response testing. 232 cpds showed <10 μM EC_{50}, further analysis based on physicochemical properties [calculated octanol-water partition

coefficient (cLogP) < 4.5; polar surface area (PSA) <110; molecular weight (MW) <500], removal of unfavourable chemical moeities and selectivity index of >10 (cytotoxicity in human hepatocytes HepG2 CC50 / *T. b. brucei* EC_{50}) lead to identification of amidobenzimidazole series.

(b) Time to kill analysis of AB1 compound. Note the concentration and time dependent killing of bloodstream form of *T. b. brucei* parasites by the AB1 compound. Data shown represent the mean ± SEM (n=3 independent biological replicates).

(c) The absolute concentrations (AC_{cure}) required to achieve sterile cure under *in vitro* conditions with incubation of compound at various time points. Note that as the time of incubation increases, ACcure reduces. Mean data from two independent biological replicates are shown.

Europe PMC Funders Author Manuscripts

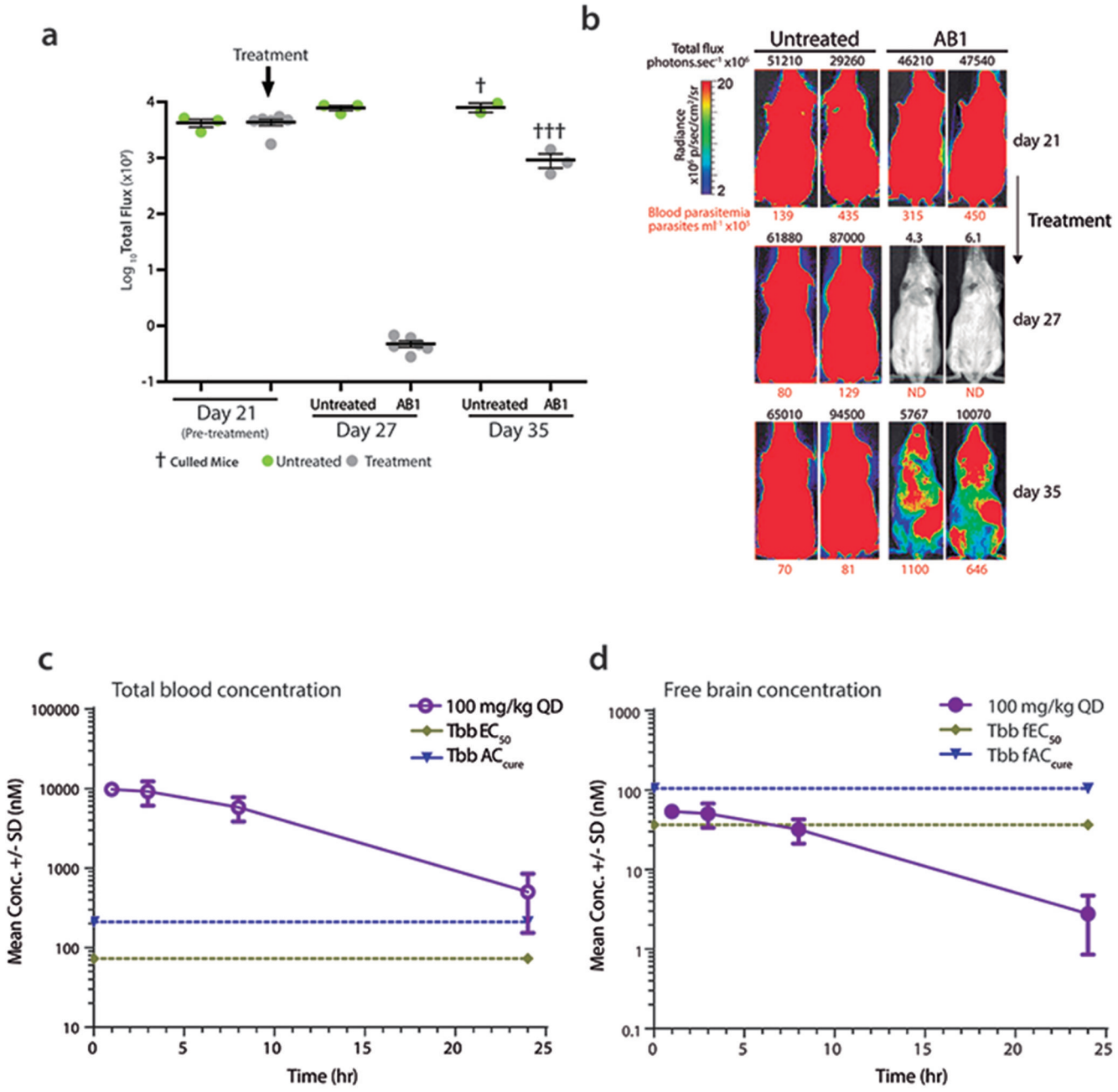

Extended Data Fig. 2. AB1 reduces parasitaemia in a GVR35 strain CNS mouse model of human African trypanosomiasis and pharmacokinetics of AB1.

(a) Whole body *in vivo* imaging of bioluminescent *T. brucei* before and after AB1 treatment; *T. b. brucei* (GVR35-VSL2) –infected mice (Day 21) were orally treated with 50 mg kg^{-1} AB1 once-daily for 7 days (n=6 mice, grey) or left untreated (n=3 mice, green); Data represent the mean ± standard deviation of each mice group, and symbols show whole body bioluminescence values for individual mice; mice were euthanized between days 27 and 35. (b) Bioluminescence images of mice showing ventral views of two representative mice from the untreated and AB1-treated groups over the full course of infection. The colour scale

indicates bioluminescent radiance in photons/sec/cm^2/sr. ND, not detected. Blood parasitemia (in parasites mL^{-1}, red font below image) and whole mouse total flux (in photons per second, black font above image) values of each animal are shown. The same two representative mice are shown for all time points.

(c) Total blood concentration of AB1 in mice at various time points after last dose from the *T. b. brucei* GVR35 strain CNS mouse model of HAT. At each time point, 3 mice were bled to collect samples, each point represents mean ± standard deviation.

(d) Free brain concentrations of AB1 compound in mice calculated by taking into consideration the brain to plasma ratio (0.5), mice plasma protein binding (94%) and rat brain tissue binding (>99%). Each point represents free brain concentrations for n=3 mice and mean ± standard deviation is shown. Note the AB1 concentrations were below *T. b. brucei* EC_{50} and AC_{cure}.

Europe PMC Funders Author Manuscripts

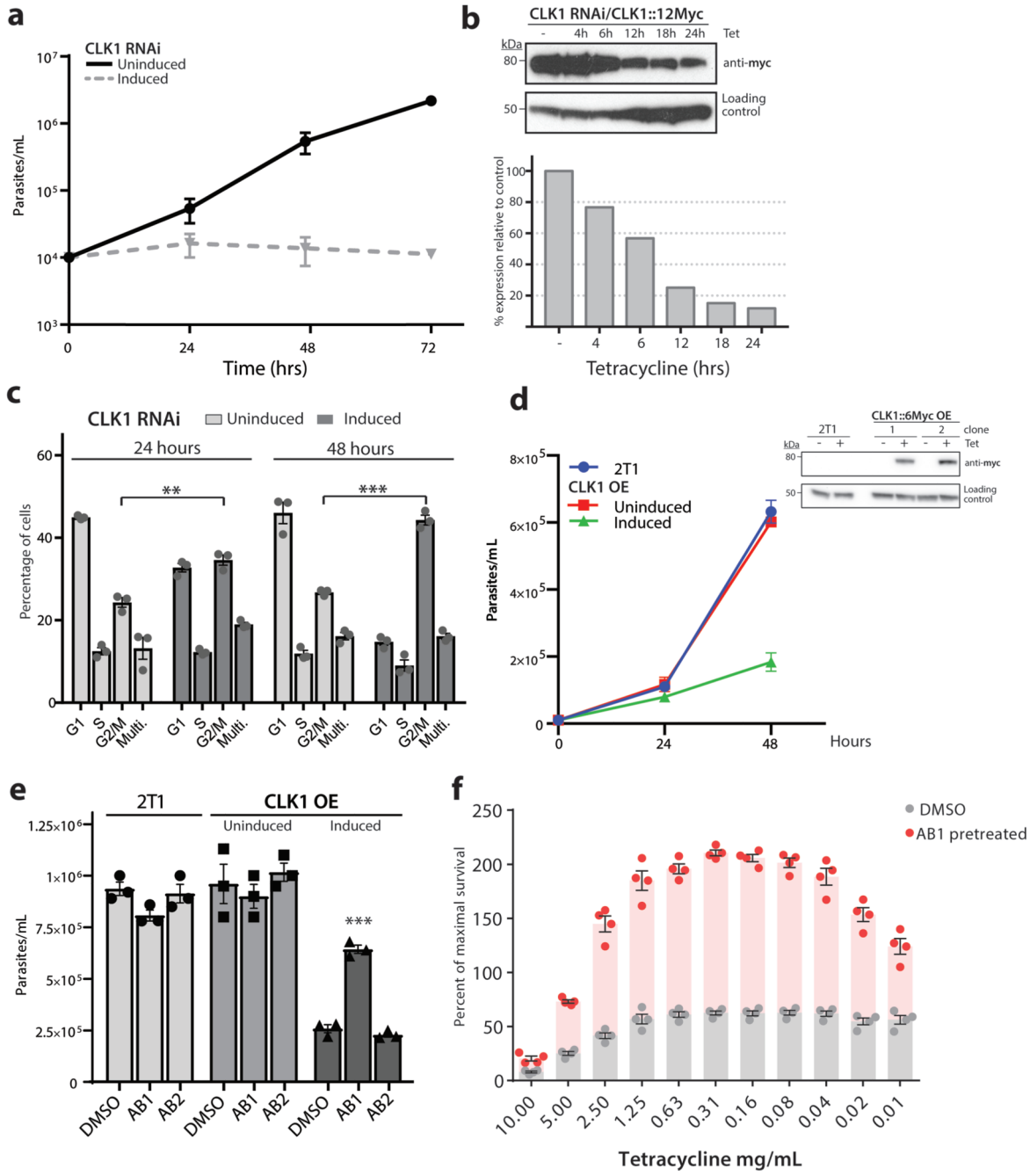

Extended Data Fig. 3. CLK1 target validation and CLK1 over- expression toxicity blockage by AB1.

(a) CLK1 depletion halts cell proliferation. Growth curves of CLK1-depleted bloodstream trypanosomes after RNAi induction with tetracycline (dashed line) is compared with uninduced (solid line) as control. Data represent the mean of two biological replicates.

(b) Efficiency of CLK1 RNAi. Upper panel: Endogenous CLK1::12-myc (predicted MW 70.5 kDa) was detected with anti-myc antibody at different points after RNAi induction. EF-1 alpha protein expression was used as the loading control. Lower panel: Mean intensity of the bands were determined from the Western blot in the upper panel. Density signal of

CLK1::12-myc was normalised to EF1α for each time point and the uninduced control and relative expression of CLK1::12-myc to uninduced control is shown. Data are representative from one of two independent biological replicates with similar results.

(c) Depletion of CLK1 induces a G2/M cell cycle arrest. Flow cytometry analysis of DNA content in CLK1-depleted cells (dark grey) and in the uninduced control (light grey) 4 and 48 h after RNAi induction with 1μg mL^{-1} tetracycline. Mean ± SEM (n=3); P values were calculated using a Two-tailed Student's t-tests comparing G2/M percentage with uninduced control where ** p =2.7 $x10^{-3}$ (24 h), *** p =1.6 $x10^{-4}$ (48 h).

(d) CLK1 overexpression impairs parasite growth. Top: 48 h growth curve of induced TbCLK1 over- expression (OE) compared with uninduced cell line and parental *T. b. brucei* 2T1 wild-type parasites. Data represent the mean ± standard deviation of three biological replicates where P- values were calculated using a Two-tailed Student's t-test; *** p= 5.9 x 10^{-5}. Bottom: CLK1-6-myc overexpression of two clones was assessed by western blot, using an anti-myc antibody. EF-1 alpha protein expression was used as the loading control.

(e) Incubation with AB1 impairs toxicity of CLK1 overexpression. Parental 2T1 and CLK1 over- expression (OE) cell lines were pre-incubated or not 18 h with 60 nM of AB1 and AB2 and then incubated with tetracycline during 48 h. Bars show the mean ± SEM (n = 3 biological replicates), and symbols represent the individual parasite counts. *** p = 1.6 $x10^{-4}$ compared to induced CLK1 OE preincubated with DMSO.

(f) CLK1 target validation using non-toxic concentrations of AB1. 24 h pre-treatment with AB1 non-toxic concentrations (60 nM) reduced the loss of fitness caused by CLK1 overexpression induced by tetracycline. Bars represent the mean ± SEM (n = 4 biological replicates) of the percentage of maximal survival in each condition, and symbols represent the individual replicates. $p < 0.001$ compared to DMSO control for all the points.

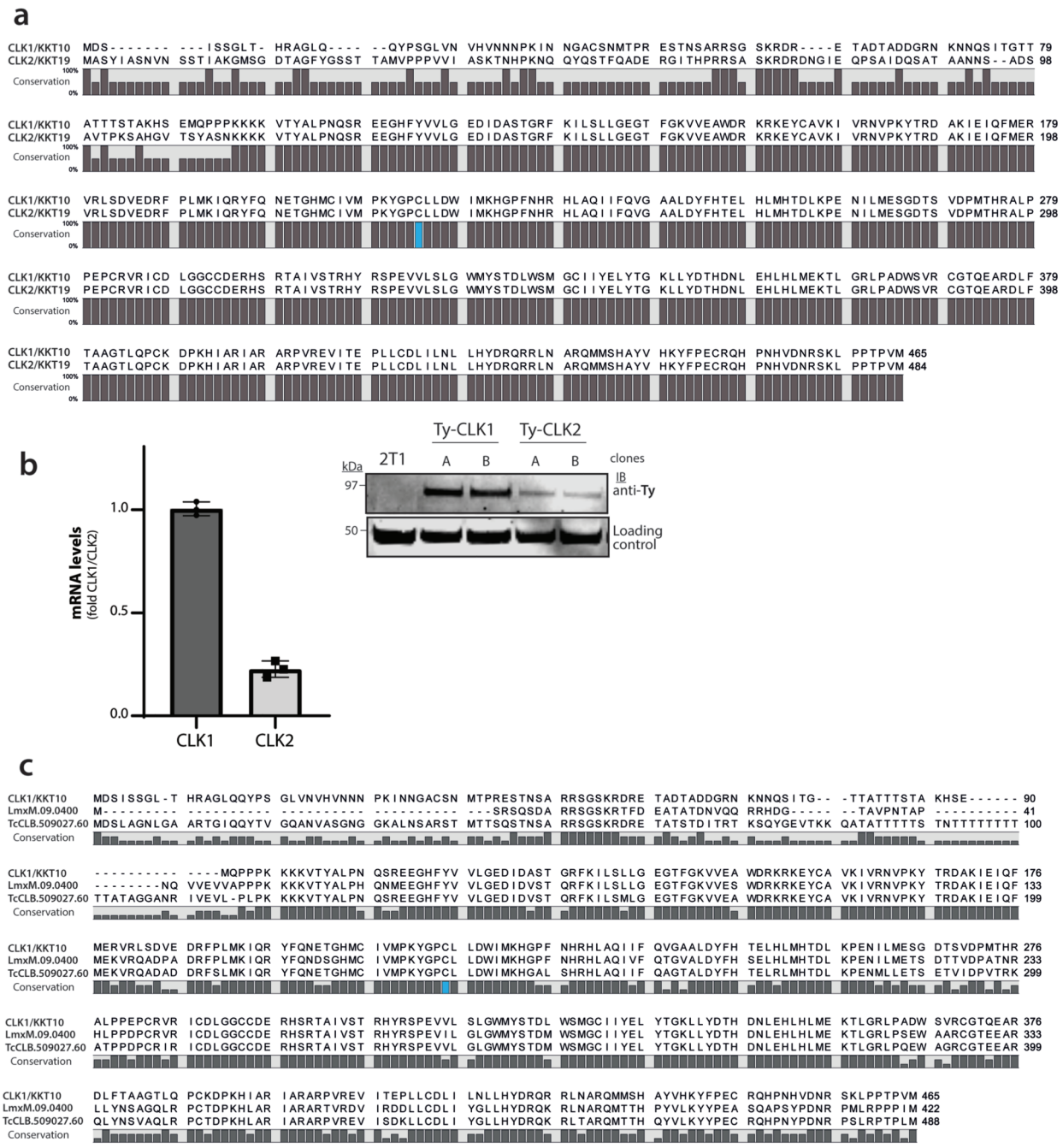

Extended Data Fig. 4. CLK1 and CLK2 protein sequence alignment and CLK1 conservation across trypanosomatids.

(a) Alignment of CLK1/KKT10 and CLK2/KKT19 protein sequence in *T. brucei*. The protein sequences of CLK1 (Tb927.11.12410) and CLK2 (Tb927.11.12420) were aligned in CLC Genomics Workbench 8 and the consensus graph is shown below the corresponding alignment. Residue Cysteine 215 is shown in blue.

(b) Left: CLK1 and CLK2 mRNA levels measured by quantitative RT-PCR (bar graphs) in the 2T1 parental cell line, using GADPH as housekeeping gene. Mean ± SEM (n=3 biological replicates). Right: Protein levels of Ty-YFP-tagged KKT10 and KKT19 were

Europe PMC Funders Author Manuscripts

assessed by western blot. Representative of two independent clones is shown. EF-1 alpha protein expression was used as the loading control.

(c) The protein sequences of CLK1/KKT10 (Tb927.11.12410) and orthologues from *Leishmania mexicana* (LmxM.09.0400) and *Trypanosoma cruzi* (TcCLB.509027.60) were aligned in CLC Genomics Workbench 8. The consensus graph is shown below the corresponding alignment. Conserved residue Cysteine 215 is shown in blue.

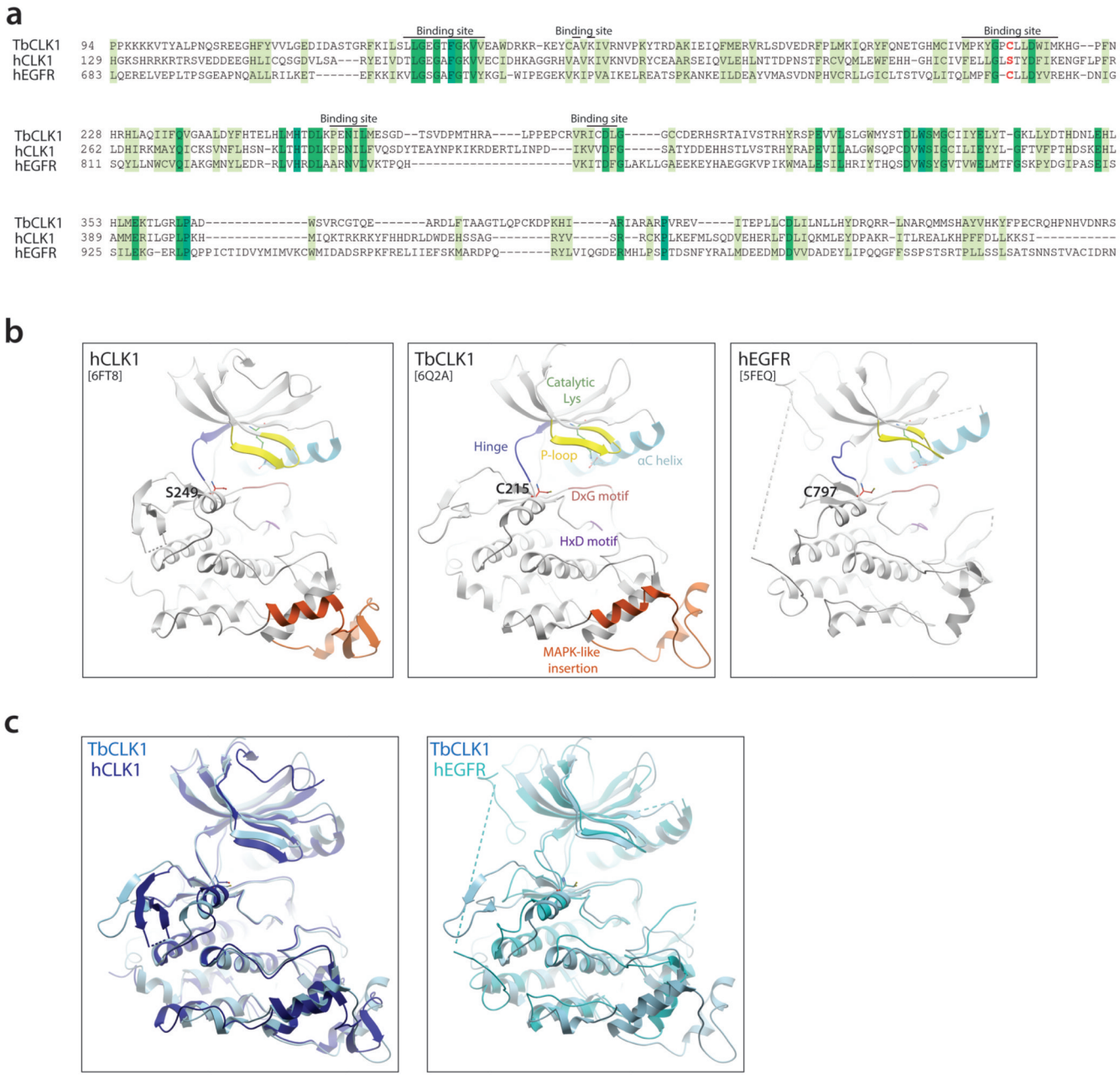

Extended Data Fig. 5. Similarity of hEGFR and CLK1 binding sites highlighting potential of AB1 to covalently bind to TbCLK1

(a) Sequence alignment of hEGFR (Uniprot id: P00533), hCLK1 (Uniprot id: P49759) and TbCLK1 show similarity in binding site residues with presence of covalent cysteine (red) in TbCLK1 explaining selectivity over hCLK1.
(b) Comparison of ribbon diagram x-ray crystal structure of hCLK1 (PDB: 6FT8), TbCLK1 (PDB: 6Q2A), and hEGFR (5FEQ). The kinase components are coloured and labelled in TbCLK1 (middle panel). Note the conservation of cysteine in the kinase domain in TbCLK1 (C215) and hEGFR (C797), whereas in the same position, hCLK1 has serine 249.
(c) An overlay of TbCLK1 with hCLK1 (left) and hEGFR (right) structures.

Europe PMC Funders Author Manuscripts

Europe PMC Funders Author Manuscripts

a

Protein	Ligand	Tm (°C) Mean ± SD	ΔTm
CLK1 WT	DMSO	41.18 ± 0.14	0.00
	AB0	41.31 ± 0.14	0.12
	AB1	53.85 ± 0.07	12.66
CLK1 C215A	DMSO	39.93 ± 0.54	0.00
	AB0	40.38 ± 0.39	0.44
	AB1	41.19 ± 0.04	1.21

b

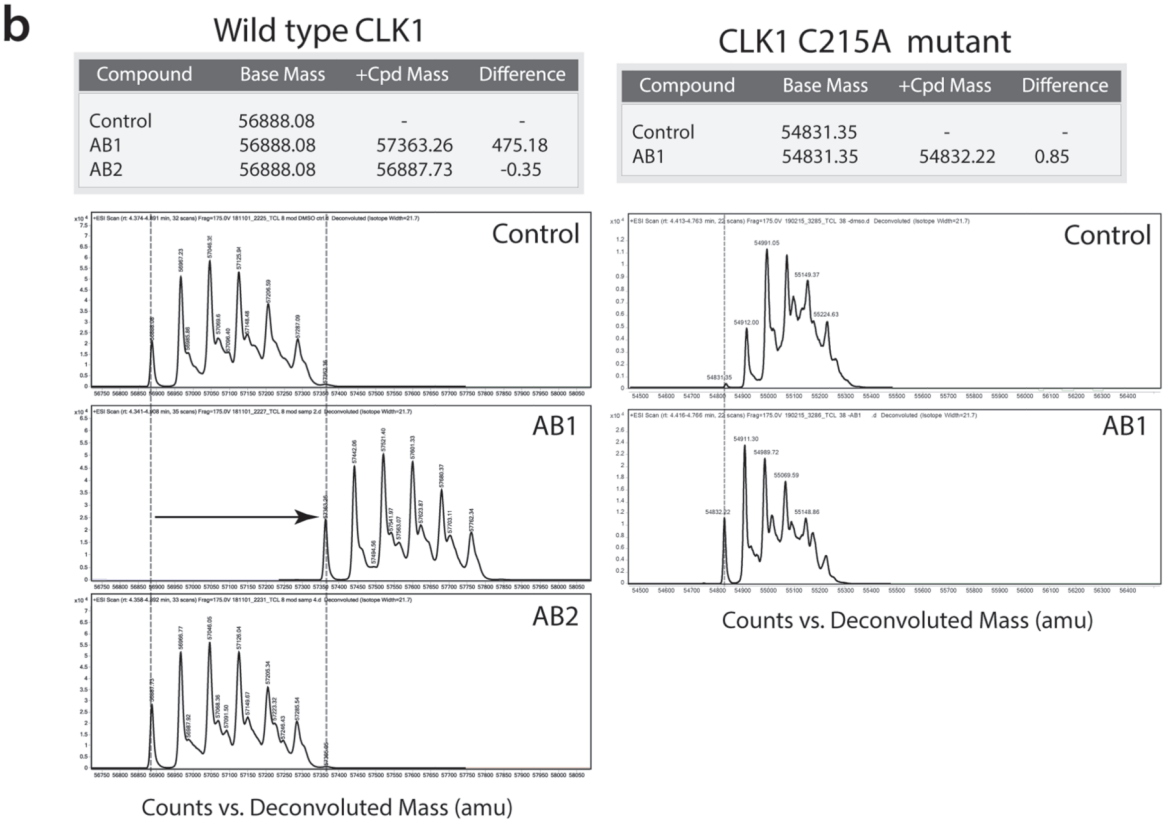

Extended Data Fig. 6. Covalent binding of AB1 to TbCLK1

(a) Summary of thermal shift assay of TbCLK1 and TbCLK1 C215A proteins incubated with DMSO, AB0 or AB1 compounds. Data represents mean ± standard deviation (n = 3 technical replicates) for ΔTm. Note the significant shift in Tm for AB1 compound bound to CLK1 but not CLK1 C215A. The Tm was calculated by fitting the fluorescence vs. temperature data to the Boltzmann equation and represents the point where half the protein is unfolded.

(b) Mass spectrum chromatograms of TbCLK1 (left) and TbCLK1 C215A proteins (right) incubated with DMSO (control), AB1 or AB2 compounds. Y-axis and X-axis represent the counts and deconvoluted Mass (amu) respectively. Calculated differences in base mass and the difference in mass after treatment is shown in the table. Note the shift in mass of 475 Da only for AB1 treatment with TbCLK1 protein, which corresponds to the mass of AB1. No shift in the mass was seen for DMSO or AB2 in both CLK1 and CLK1 C215A protein. Treatment of CLK1 C215A with AB1 also did not result in shift in mass, clearly showing covalent interaction of the Michael acceptor with C215 of TbCLK1 (n=1).

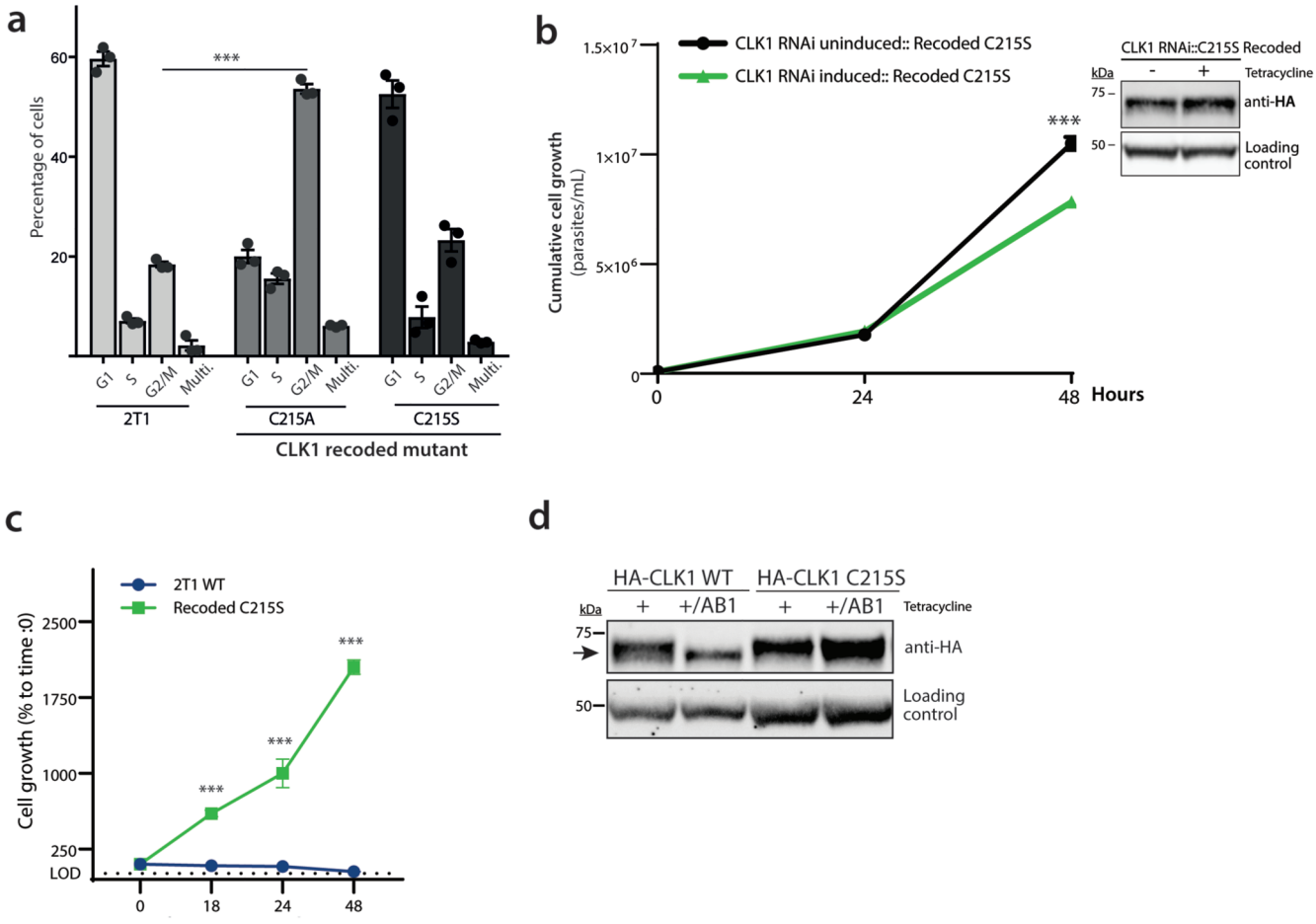

Extended Data Fig. 7. Expression of CLK1 C215A mutant in *T. brucei*

a) Expression of CLK1 C215A results in a G2/M cell cycle arrest. Induction of recoded CLK1 C215A and C215S mutants were expressed for 24 h with tetracycline and cell cycle distribution was determined by flow cytometry and compared with 2T1 parental cell line. Bars represent the mean ± SEM (n = 3 independent experiments). P values were calculated using a Two-tailed Student's t-test comparing G2/M phase with parental 2T1 control where *** $p = 6.0 \times 10^{-6}$.

b) Constitutive expression of recoded CLK1 C215S halts CLK1 RNAi growth inhibition. Parasites were induced or not with 1μg mL^{-1} tetracycline at 1 x 10^5 parasites ml^{-1} and daily diluted up to 48 h, where ~ 25% reduction in parasite growth was observed. Data represent

Europe PMC Funders Author Manuscripts

Europe PMC Funders Author Manuscripts

mean ± SEM (n= 4 technical replicates) showing cumulative cell growth across time. The P values were calculated using a two-tailed Student's t-test comparing the recoded mutant with parental uninduced control where *** p= 7.9 x 10^{-4}. A representative Western blot of expression of recoded CLK1 C215S mutant is shown in the right panel. The expression of recoded CLK1 was detected using an anti-HA antibody. EF-1 alpha protein expression was used as the loading control.

c) CLK1 C215S mutant impairs the parasite growth effect of 48 h with 5x AB1 EC_{50} treatment. Growth curve of parasites expressing recoded CLK1 C215S (green) and parental 2T1 cell line (blue) (5 x 10^5 parasites ml^{-1}) treated with 5x AB1 EC_{50} for 48 h. Data represents mean ± SEM (n=3 technical replicates). *** P values were calculated using a Two-tailed Student's t-test comparing the recoded CLK1 C215S cell line with parental control at each time point, 18 h (p = 3.0 x 10^{-6}), 24h (p = 1.1 x 10^{-4}) and 48 h (p = 2.5 x10^{-7}).

d) *T. brucei* expressing recoded HA-tagged TbCLK1 and C215S mutant were incubated induced or not with 1 μg mL^{-1} tetracycline for 24 h and then treated with 5x EC_{50} AB1 for 6 h. The expression of recoded CLK1 was detected using an anti-HA antibody. EF-1α protein expression was used as the loading control. The size shift of CLK1 is showed with an arrow. Data shown is representative from one of the three biological replicates with similar results.

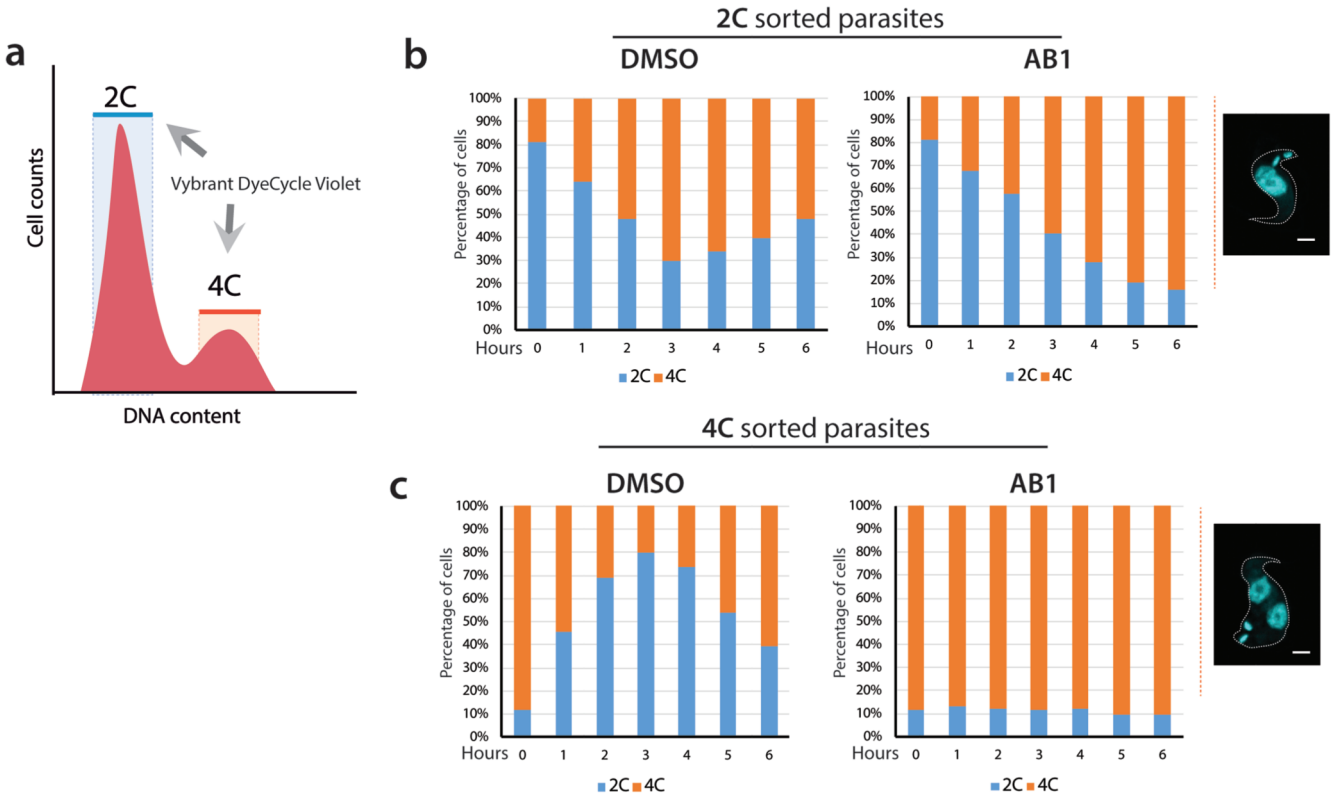

Extended Data Fig. 8. Cell cycle analysis of synchronized *T. brucei* after treatment with AB1.

(a) Diagram of 2C (blue) and 4C (orange) cell cycle synchronised bloodstream form *T. brucei* using Vybrant DyeCycle Violet-based cell sorting. The selected area shows those cells that were gated for sorting.

(b - c) After release, 2C and 4C synchronised parasites were treated or not with 5x EC_{50} AB1. Then, cell samples were collected every hour for DNA flow cytometry analysis of 2C (in blue) and 4C (orange) populations, up to 6 hours. A representative micrograph after 6 hours of treatment is also provided in each condition. Scale bar, 2μm. The data are representative of two biological experiments.

Supplementary Material

Refer to Web version on PubMed Central for supplementary material.

Acknowledgments

This work was supported by the Wellcome Trust (069712, 103024 and 108517). JCM is a Wellcome Trust Investigator (200807). MPB and JCM are part of the Wellcome Centre of Integrative Parasitology (104111/Z/14/Z). We thank our colleagues in The Bioscience Technology Facility of University of York who provided insight and expertise that greatly assisted our microscopy and flow cytometry research. We thank Gerald Lelais, Vanessa Manoharan, Rima Palkar, Vivian Lim, Christian Noble and Wan Kah Fei for their technical support.

Data availability

All the source data used for generating Figures 1-5 and Extended Data Figs. 1-8 have been provided as source data. Any other data that support the findings of this study are available from the corresponding author upon request. *Trypanosoma brucei* CLK1 kinase domain in complex with covalent aminobenzimidazole inhibitor AB1 is annotated in PDB with an accession number 6Q2A.

Bibliography

1. World Health Organization. Integrating neglected tropical diseases into global health and development: fourth World Health Organization report on neglected tropical diseases. apps.who.int; 2017.
2. Mesu VKBK, et al. Oral fexinidazole for late-stage African Trypanosoma brucei gambiense trypanosomiasis: a pivotal multicentre, randomised, non-inferiority trial. Lancet. 2018; 391:144–154. [PubMed: 29113731]
3. Dickie EA, et al. New drugs for human african trypanosomiasis: A twenty first century success story. TropicalMed. 2020; 5
4. Khare S, et al. Proteasome inhibition for treatment of leishmaniasis, Chagas disease and sleeping sickness. Nature. 2016; 537:229–233. [PubMed: 27501246]
5. Wyllie S, et al. Cyclin-dependent kinase 12 is a drug target for visceral leishmaniasis. Nature. 2018; 560:192–197. [PubMed: 30046105]
6. Rao SPS, et al. Drug discovery for kinetoplastid diseases: future directions. ACS Infect Dis. 2019; 5:152–157. [PubMed: 30543391]
7. Myburgh E, et al. In vivo imaging of trypanosome-brain interactions and development of a rapid screening test for drugs against CNS stage trypanosomiasis. PLoS Negl Trop Dis. 2013; 7:e2384. [PubMed: 23991236]
8. Lelais G, et al. Discovery of (R,E)-N-(7-Chloro-1-(1-[4-(dimethylamino)but-2-enoyl]azepan-3-yl)-1H-benzo[d]imidazol-2-yl)-2-methylisonicotinamide (EGF816), a Novel, Potent, and WT Sparing Covalent Inhibitor of Oncogenic (L858R, ex19del) and Resistant (T790M) EGFR Mutants for the Treatment of EGFR Mutant Non-Small-Cell Lung Cancers. J Med Chem. 2016; 59:6671–6689. [PubMed: 27433829]

9. Parsons M, Worthey EA, Ward PN, Mottram JC. Comparative analysis of the kinomes of three pathogenic trypanosomatids: Leishmania major, Trypanosoma brucei and Trypanosoma cruzi. BMC Genomics. 2005; 6:127. [PubMed: 16164760]
10. Begolo D, Erben E, Clayton C. Drug target identification using a trypanosome overexpression library. Antimicrob Agents Chemother. 2014; 58:6260–6264. [PubMed: 25049244]
11. McNamara CW, et al. Targeting Plasmodium PI(4)K to eliminate malaria. Nature. 2013; 504:248–253. [PubMed: 24284631]
12. Moeslein FM, Myers MP, Landreth GE. The CLK family kinases, CLK1 and CLK2, phosphorylate and activate the tyrosine phosphatase, PTP-1B. J Biol Chem. 1999; 274:26697–26704. [PubMed: 10480872]
13. Jones NG, et al. Regulators of Trypanosoma brucei cell cycle progression and differentiation identified using a kinome-wide RNAi screen. PLoS Pathog. 2014; 10:e1003886. [PubMed: 24453978]
14. Akiyoshi B, Gull K. Discovery of unconventional kinetochores in kinetoplastids. Cell. 2014; 156:1247–1258. [PubMed: 24582333]
15. Nishino M, Choy JW, Gushwa NN, Oses-Prieto JA. Hypothemycin, a fungal natural product, identifies therapeutic targets in Trypanosoma brucei. Elife. 2013
16. Liu Q, et al. Developing irreversible inhibitors of the protein kinase cysteinome. Chem Biol. 2013; 20:146–159. [PubMed: 23438744]
17. Westhorpe FG, Straight AF. Chromosome segregation: reconstituting the kinetochore. Curr Biol. 2016; 26:R1242–R1245. [PubMed: 27923136]
18. D'Archivio S, Wickstead B. Trypanosome outer kinetochore proteins suggest conservation of chromosome segregation machinery across eukaryotes. J Cell Biol. 2017; 216:379–391. [PubMed: 28034897]
19. Kabani S, Waterfall M, Matthews KR. Cell-cycle synchronisation of bloodstream forms of Trypanosoma brucei using Vybrant DyeCycle Violet-based sorting. Mol Biochem Parasitol. 2010; 169:59–62. [PubMed: 19729042]
20. Torrie LS, et al. Identification of inhibitors of an unconventional Trypanosoma brucei kinetochore kinase. PLoS One. 2019; 14:e0217828. [PubMed: 31150492]
21. Ishii M, Akiyoshi B. Characterization of unconventional kinetochore kinases KKT10/19 in Trypanosoma brucei. J Cell Sci. 2020; doi: 10.1242/jcs.240978
22. Mackey ZB, Koupparis K, Nishino M, McKerrow JH. High-throughput analysis of an RNAi library identifies novel kinase targets in Trypanosoma brucei. Chem Biol Drug Des. 2011; 78:454–463. [PubMed: 21668652]
23. Roskoski R. Properties of FDA-approved small molecule protein kinase inhibitors. Pharmacol Res. 2019; 144:19–50. [PubMed: 30877063]
24. Wyllie S, et al. Preclinical candidate for the treatment of visceral leishmaniasis that acts through proteasome inhibition. Proc Natl Acad Sci USA. 2019; 116:9318–9323. [PubMed: 30962368]
25. Alam MM, et al. Validation of the protein kinase PfCLK3 as a multistage cross-species malarial drug target. Science. 2019; 365
26. van Hooff JJ, Tromer E, van Wijk LM, Snel B, Kops GJ. Evolutionary dynamics of the kinetochore network in eukaryotes as revealed by comparative genomics. EMBO Rep. 2017; 18:1559–1571. [PubMed: 28642229]
27. Duncan SM, et al. Conditional gene deletion with DiCre demonstrates an essential role for CRK3 in Leishmania mexicana cell cycle regulation. Mol Microbiol. 2016; 100:931–944. [PubMed: 26991545]
28. Buckner FS, Verlinde CL, La Flamme AC, Van Voorhis WC. Efficient technique for screening drugs for activity against Trypanosoma cruzi using parasites expressing beta-galactosidase. Antimicrob Agents Chemother. 1996; 40:2592–2597. [PubMed: 8913471]
29. Alsford S, Kawahara T, Glover L, Horn D. Tagging a T. brucei RRNA locus improves stable transfection efficiency and circumvents inducible expression position effects. Mol Biochem Parasitol. 2005; 144:142–148. [PubMed: 16182389]
30. Dean S, Sunter JD, Wheeler RJ. TrypTag.org: A Trypanosome Genome-wide Protein Localisation Resource. Trends Parasitol. 2017; 33:80–82. [PubMed: 27863903]

31. Kaiser M, et al. Antitrypanosomal activity of fexinidazole, a new oral nitroimidazole drug candidate for treatment of sleeping sickness. Antimicrob Agents Chemother. 2011; 55:5602–5608. [PubMed: 21911566]
32. Alsford S, Horn D. Single-locus targeting constructs for reliable regulated RNAi and transgene expression in Trypanosoma brucei. Mol Biochem Parasitol. 2008; 161:76–79. [PubMed: 18588918]
33. Thuita JK, et al. Efficacy of the diamidine DB75 and its prodrug DB289, against murine models of human African trypanosomiasis. Acta Trop. 2008; 108:6–10. [PubMed: 18722336]
34. Waters NJ, Jones R, Williams G, Sohal B. Validation of a rapid equilibrium dialysis approach for the measurement of plasma protein binding. J Pharm Sci. 2008; 97:4586–4595. [PubMed: 18300299]
35. Kalvass JC, Tess DA, Giragossian C, Linhares MC, Maurer TS. Influence of microsomal concentration on apparent intrinsic clearance: implications for scaling in vitro data. Drug Metab Dispos. 2001; 29:1332–1336. [PubMed: 11560877]
36. Winter G. Xia2 : an expert system for macromolecular crystallography data reduction. J Appl Crystallogr. 2010; 43:186–190.
37. Kabsch WXDS. Acta Crystallogr Sect D, Biol Crystallogr. 2010; 66:125–132. [PubMed: 20124692]
38. Evans PR, Murshudov GN. How good are my data and what is the resolution? Acta Crystallogr Sect D, Biol Crystallogr. 2013; 69:1204–1214. [PubMed: 23793146]
39. McCoy AJ, et al. Phaser crystallographic software. J Appl Crystallogr. 2007; 40:658–674. [PubMed: 19461840]
40. Walter A, et al. Molecular structures of cdc2-like kinases in complex with a new inhibitor chemotype. PLoS One. 2018; 13:e0196761. [PubMed: 29723265]
41. Adams PD, et al. PHENIX: a comprehensive Python-based system for macromolecular structure solution. Acta Crystallogr Sect D, Biol Crystallogr. 2010; 66:213–221. [PubMed: 20124702]
42. Emsley P, Lohkamp B, Scott WG, Cowtan K. Features and development of Coot. Acta Crystallogr Sect D, Biol Crystallogr. 2010; 66:486–501. [PubMed: 20383002]

Europe PMC Funders Author Manuscripts

Europe PMC Funders Author Manuscripts

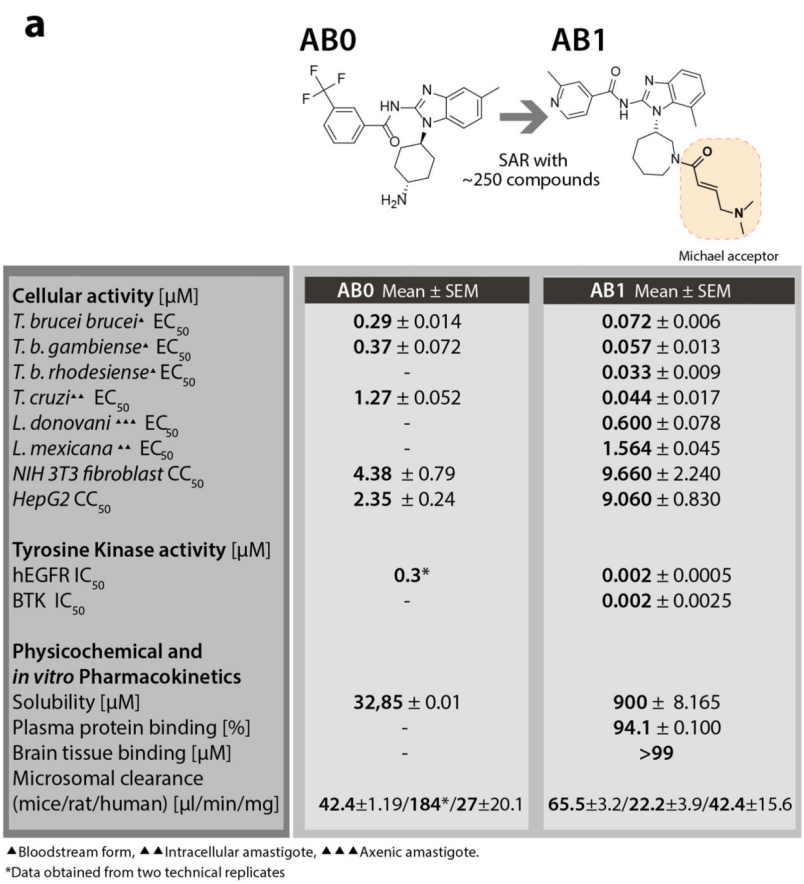

	AB0 Mean ± SEM	AB1 Mean ± SEM
Cellular activity [µM]		
T. brucei brucei▲ EC_{50}	**0.29** ± 0.014	**0.072** ± 0.006
T. b. gambiense▲ EC_{50}	**0.37** ± 0.072	**0.057** ± 0.013
T. b. rhodesiense▲ EC_{50}	-	**0.033** ± 0.009
T. cruzi▲▲ EC_{50}	**1.27** ± 0.052	**0.044** ± 0.017
L. donovani ▲▲▲ EC_{50}	-	**0.600** ± 0.078
L. mexicana ▲▲ EC_{50}	-	**1.564** ± 0.045
NIH 3T3 fibroblast CC_{50}	**4.38** ± 0.79	**9.660** ± 2.240
HepG2 CC_{50}	**2.35** ± 0.24	**9.060** ± 0.830
Tyrosine Kinase activity [µM]		
hEGFR IC_{50}	**0.3***	**0.002** ± 0.0005
BTK IC_{50}	-	**0.002** ± 0.0025
Physicochemical and *in vitro* Pharmacokinetics		
Solubility [µM]	**32,85** ± 0.01	**900** ± 8.165
Plasma protein binding [%]	-	**94.1** ± 0.100
Brain tissue binding [µM]	-	**>99**
Microsomal clearance (mice/rat/human) [µl/min/mg]	**42.4**±1.19/**184***/**27**±20.1	**65.5**±3.2/**22.2**±3.9/**42.4**±15.6

▲Bloodstream form, ▲▲Intracellular amastigote, ▲▲▲Axenic amastigote.
*Data obtained from two technical replicates

Fig. 1. Pan kinetoplastid activity of amidobenzimidazole (AB) series.

(a) Structure, anti-kinetoplastid parasite activity, cytotoxicity, tyrosine kinase inhibition and *in vitro* pharmacokinetics of AB0 and AB1. $EC_{50,}$ and CC_{50} represent half-maximum growth inhibition concentration. hEGFR: human epidermal growth factor receptor enzyme. BTK: Bruton's tyrosine kinase. IC_{50} represents half-maximum enzyme inhibition concentration. All the cellular and biochemical data presented were generated with minimum of n=2 or more independent biological replicates (each biological replicate had n=2 technical replicates). All physicochemical and in vitro pharmacokinetics experiments were carried out with at least n = 4 technical replicates (except for rat microsomal clearance for AB0, which had n =2 technical replicates).

(b) Structure activity relationship of amidobenzimidazoles. Each dot represents one compound. Compounds with the Michael acceptor (orange circles) were more potent against *T. b. brucei* (Tbb pEC_{50}) and had better lipophilic efficiency (clogP, calculated octanol-water partition coefficient) compared to non-Michael acceptor compounds (blue circles). AB0 (dark blue) and AB1 (dark orange). The Tbb pEC_{50} data are the negative logarithm of 50% growth inhibition of bloodstream form of *T. b. brucei* (minimum n = 2 biological replicates). The compounds on the left side of the two slanted dotted lines represent lipophilic ligand efficiency (LipE) of 3 and 4. The compounds above two horizontal dotted lines have EC_{50} of 1000 and 100 nM against bloodstream form *T. b. brucei*.

(c) *In vivo* activity of AB1 in a haemolymphatic mouse model for human African trypanosomiasis (untreated control group, mice = 4; all the other experimental groups, mice = 6). Each group of mice were infected with *T. b. brucei* and 3 days post infection, mice were treated with varying concentration of AB1 for 4 days once daily and monitored for relapse in parasitemia over a period of 31 days. Cure plot (Kaplan–Meier plot) showing percentage of animals cured over time are shown. Note the dose dependent activity of AB1, achieving complete cure at 50 mg kg^{-1} once daily dose (in violet).

Europe PMC Funders Author Manuscripts

Europe PMC Funders Author Manuscripts

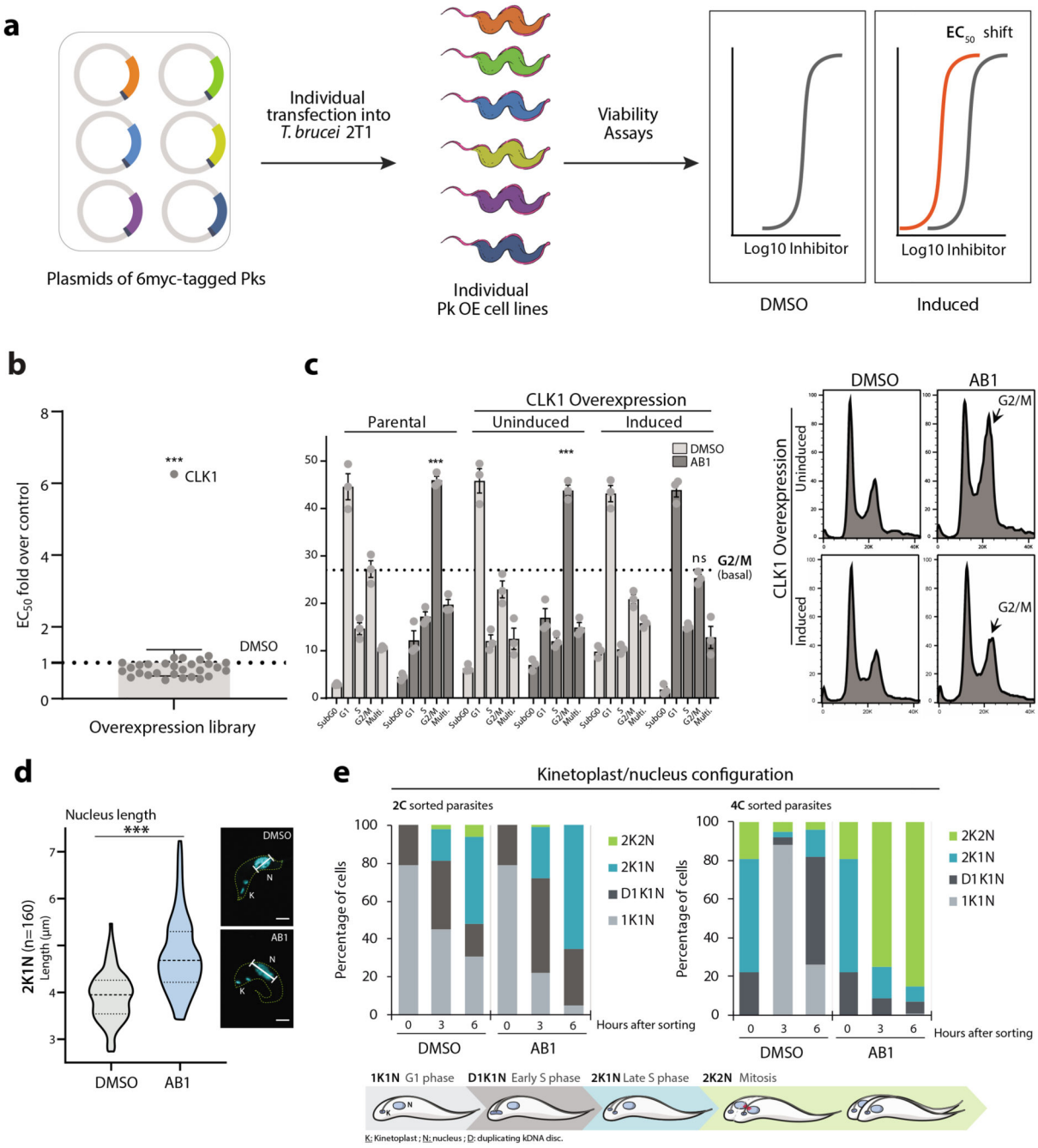

Fig. 2. Identification of CLK1 as the molecular target for the AB series.

(a) Inducible overexpression (OE) of essential protein kinases (PKs) and target deconvolution approach for the AB series. Schematic representation of the experimental workflow: 6-myc OE plasmids, each containing a specific protein kinase tagged with six myc epitopes, were individually transfected into 2T1 bloodstream form *T. b. brucei* (VSG221 expressing, Tagged, clone 1). Viability of induced individual *T. b. brucei* OE lines after treatment was assessed by measuring the conversion of resazurin (Alamar blue) to resorufin.

(b) AB1 half-maximal effective concentration (EC_{50}) was analysed from twenty-nine essential individual protein kinase over-expression cell lines (dark grey circles). The graph represents EC_{50} fold change over the parental cell line (*T. b. brucei* 2T1 cell line, DMSO) (light grey shade box), where overexpression of CLK1 confers resistance to AB1. The grey bar represents the EC_{50} average of all cell lines over control. Box error bars represent the library mean with 95% of confidence interval of two biological replicates of the library and CLK1 (n = 4 biological replicates). P-value was calculated using two-tailed Student's t-tests comparing CLK1 OE with parental cell line where *** p-value = 5×10^{-5}.

(c) CLK1 over-expression confers resistance to AB1-induced cell cycle arrest. CLK1 over-expression was induced or not with tetracycline for 18 h, and cells then incubated for 6 h with 5x AB1 EC_{50} (dark grey bars); the 2T1 cell line was a parental control. Cell cycle distribution was determined by flow cytometry. Left: dotted line represents (basal) G2/M untreated average and *** represents a p-value =1.2×10^{-4} (2T1 untreated vs AB1), p-value = 5.8×10^{-4} (CLK1 OE uninduced vs AB1), and not signficant (ns) p-value = 0.02 (CLK1 OE induced vs AB1). P-value was calculated using two-tailed Student's t-test. Error bars represent mean ± SEM of three biological replicates, Right: representative cell cycle profile histogram of cells stained with propidium iodide showing G2/M cell cycle accumulation (arrow).

(d) Violin plot of average length (μm) of the nuclei from parasites treated (blue) or not (grey) with AB1 (n=160 2K1N parasites, *** p-value = 3.9×10^{-26}). Dashed line represents the mean value, and dotted lines indicate both quartiles (25^{th} & 75^{th}). P-value was calculated using unpaired two-tailed Student's t-test. Right: Example of a cell stained with DAPI (cyan) from each condition, where N= nucleus, K= Kinetoplast. Scale bar, 2μm.

(e) Cell cycle analysis of synchronized *T. b. brucei* after treatment with AB1. Top: Kinetoplast/nucleus configuration of 2C and 4C synchronized parasites, treated or not with 5x EC_{50} AB1 was quantified by DAPI staining at the indicated points (n=200 cells). K = kDNA, N = nucleus, D = duplicating kDNA. Bottom: Schematic representation of *T. brucei* kinetoplast/nucleus configuration through the cell cycle.

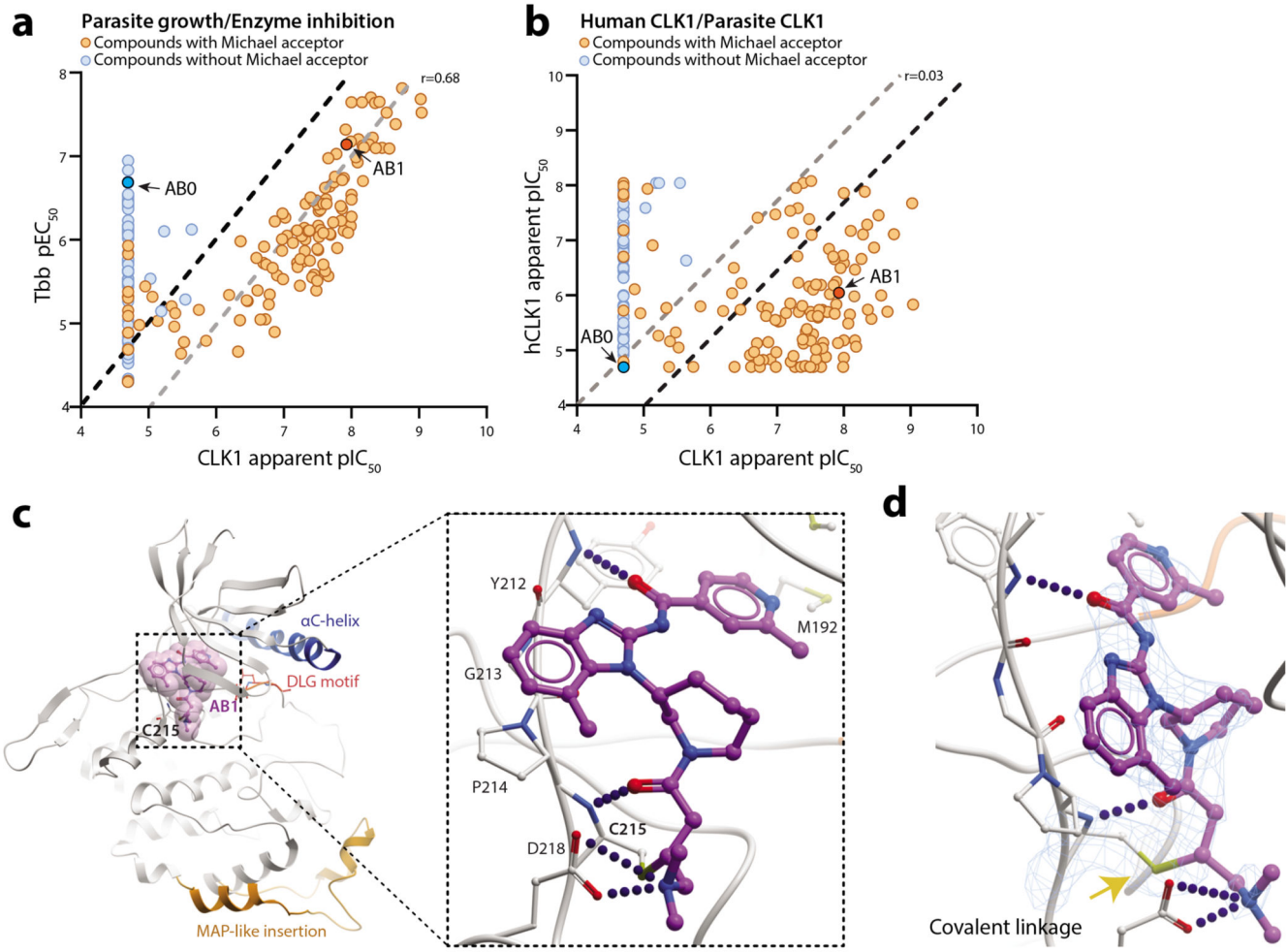

Fig. 3. Mechanism of CLK1 inhibition by AB1

(a) Positive correlation between inhibition of recombinant *T. brucei* CLK1 enzyme (apparent pIC_{50}) and growth inhibition (pEC_{50}) of *T. b. brucei* bloodstream form parasites with AB series compounds (n=260; Pearson correlation coefficient (r) = 0.68. Presence (orange) or absence (blue) of Michael acceptor pharmacophore is shown, highlighting AB1 (dark orange) and AB0 (dark blue). Black dash line represents equimolar potency and grey dash line represents 10-fold higher potency for CLK1 pIC_{50} compared to Tbb pEC_{50}.

(b)Lack of correlation between inhibition of recombinant human CLK1 (hCLK1) and recombinant *T. brucei* CLK1 enzyme (apparent pIC_{50}) with AB compound series (n=228; Pearson correlation coefficient (r) = 0.03). Majority of compounds showed > 10-fold selectivity against TbCLK1 compared to hCLK1. Presence (orange) or absence (blue) of Michael acceptor pharmacophore is shown, highlighting AB1 (dark orange) and AB0 (dark blue). Grey dash line represents equimolar potency and black dash line represents 10-fold higher potency for CLK1 pIC_{50} compared to hCLK1 pIC_{50}.

(c) Crystal structure of the *T. brucei* CLK1 kinase domain (V117-M465) in a covalent thioether bond with AB1 at C215 (PDB: 6Q2A). The CLK1 kinase domain is shown in grey, with a blue αC helix, and the side chains of the DFG motif (DLG in CLK1) shown as sticks. Inhibitor AB1 is shown as ball and sticks with carbon coloured purple, oxygen coloured red

and nitrogen coloured blue. A semi-transparent representation of AB1 van der Waals surfaces are shown in magenta. Inset depicts the detailed view of the interactions of AB1. Hydrogen bonds and salt bridge are shown as dotted blue line. MAP-like insertion is showed in orange.

(d) Omit 2Fo-Fc map of AB1/C215 at 2.6Å resolution contoured at 2σ. Hydrogen bonds and salt bridge between the AB1 molecule and *T. brucei* bCLK1 are drawn as blue lines. Covalent bond indicated by yellow arrow.

Europe PMC Funders Author Manuscripts

Europe PMC Funders Author Manuscripts

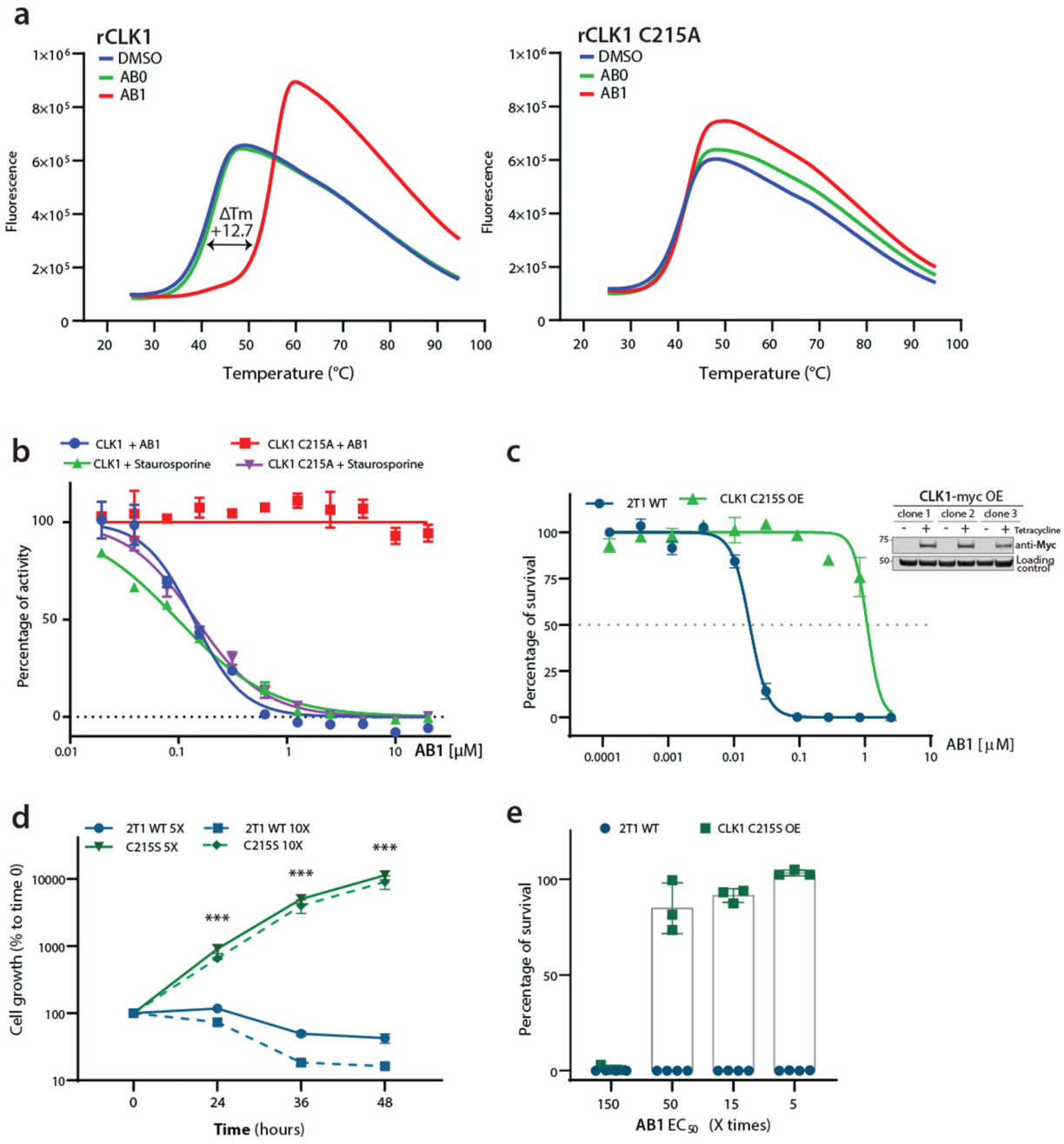

Fig. 4. CLK1 is the primary target for AB1 in bloodstream form trypanosomes

(a) AB1 binding to CLK1, as probed via differential scanning fluorimetry (DSF). Thermal unfolding of CLK1 is monitored by SYPRO Orange. CLK1 WT (left) and CLK1 C215A (right) recombinant protein in the presence of AB0 (green), AB1 (red) or DMSO (blue) as a reference. Data from one representative experiment, out of three independent experiment with similar results, are shown. Note the shift in Tm (melting temperature of protein) for CLK1 in presence of AB1 compound.

(b) Expression of *T. brucei* CLK1 C215A mutant is resistant to AB1. Dose-response curves of apparent AB1 and staurosporine IC_{50} of recombinant WT *T. brucei* CLK1 and C215A mutant. Response to 3-fold serial dilutions of each compound were assessed as described in methods. Each data point represents the mean of two technical replicates.

(c) Overexpression of CLK1 C215S mutant confers > 60-fold EC_{50} shift to AB1. CLK1 C215S mutation (green) was overexpressed in the parental *T. b. brucei* 2T1 cell line and AB1 half-maximal effective concentration (EC_{50}) was determined after 72 h and compared with *T. b. brucei* 2T1 WT parental cell line (blue). Data represent mean ± SEM of three independent biological experiments. Inset: Tetracycline inducible over-expression of CLK1-myc was assessed for three clones by western blot, using an anti-myc antibody. EF1α was used as the loading control.

(d) Overexpression of CLK1 C215S mutant impairs the parasite growth effect of AB1 treatment. Parasites overexpressing CLK1 C215S (green) and parental *T. b. brucei* 2T1 cell line (blue) were treated with 5x (line) or 10x AB1 EC_{50} (dashed line) during 48 h. Mean ± SEM (n=3) is shown. Data represent the mean of the percentage of cell growth relative to time=0 h (1.5×10^4 parasites ml^{-1}). P values were calculated using a two-tailed Student's t-test comparing with parental control where *** represent the P-values of 24 h (p-value = 5.4×10^{-4}), 48 h (p-value = 3.4 x 10-4), and 72 h (p-value = 3.3×10^{-4}) after treatment with 5x AB1 EC_{50}, and 24 h (p-value = 9.9×10^{-7}), 48 h (p-value = 1.7×10^{-3}), and 72 h (p-value = 1.6×10^{-3}) for 10x AB1 EC_{50} treatment.

(e) Percentage of survival of parasites exposed to 5-150x AB1 EC_{50} fold range. Parental *T. b. brucei* 2T1 control (blue) and CLK1 C215S mutant (green) (2×10^3 parasites ml-^{1}) were exposed for 72 h to 5, 15, 50, and 150-fold AB1 EC_{50}. Survival was calculated by using CellTiter-Glo® luminescent cell viability assay. Data represent the mean ± SEM of percentage of survival. (C215S mutant n=3, Parental 2T1 n=4).

Europe PMC Funders Author Manuscripts

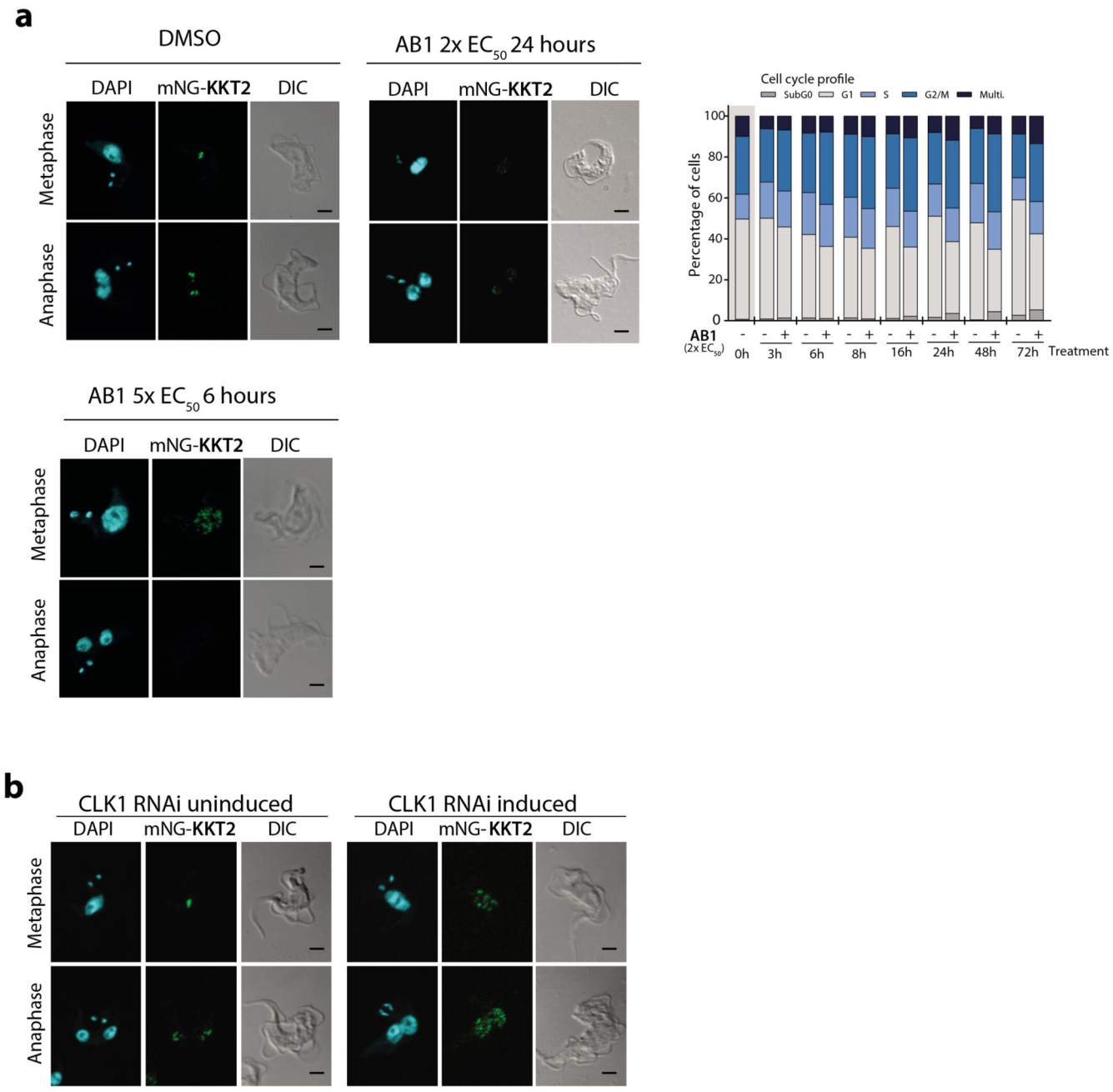

Fig. 5. CLK1 inhibition impairs inner kinetochore dynamics.

(a) Localization of kinetochore protein KKT2 after CLK1 inhibition by AB1. Parasites were incubated or not for 24 h with 2x EC_{50} (upper panel) or 6 h with 5 x EC_{50} AB1 (lower panel). Representative fluorescence micrographs, showing bloodstream form parasites endogenously expressing N-terminal mNeonGreen (mNG) tagged KKT2. Cells in metaphase and anaphase are shown. Cells were counterstained with DAPI to visualize DNA (cyan). The right panel shows the Nomarsky (DIC) corresponding images. Scale bar, 2μm. Upper right panel shows cell cycle progression after treatment with 2x EC_{50} AB1 for 72 h.

Data are representative from one of three independent biological replicates with similar results.

(b) Localization of KKT2 after CLK1 depletion by RNAi. Representative fluorescence micrographs, showing 24 h induction of CLK1 RNAi in bloodstream form parasites endogenously expressing N-terminal mNeonGreen (mNG) labelled KKT2, compared with not induced control cells in metaphase and anaphase are shown. Cells were counterstained with DAPI to visualize DNA (cyan). The right panel shows the Nomarsky (DIC) corresponding images. Scale bar, 2μm. Data are representative from one of three independent biological replicates with similar results.

Europe PMC Funders Author Manuscripts